NTNU – Trondheim
Norwegian University of
Science and Technology

Norwegian University of Science and Technology

Master's Thesis

Structural strength of work boats and high speed crafts with pre-fabricated, floating panels in aluminum

---

Author:
Lars Johan Mong

Supervisor:
Prof. Jørgen Amdahl

June, 2011

Abstract

This thesis evaluates some relevant aspects related to structural integrity for work boats and high speed vessels with floating frames. This structural design is expected to significantly reduce the building cost, but it is also expected to reduce the structural strength of the vessel. A model of a modified version of the JumboCat 60 (JC60) with floating frames is used as a recurring example in the calculations.

As of date, the use of floating frames in not acknowledge by the classification societies. The traditional version of the JC60 is however classified according to the DNV HSLC rules, and it is shown that the scantlings for the floating frame version exceeds the minimum requirements in the rules.

Finite element models of the traditional and the floating frame version of the JC60 has been developed. These has been analysed for three different load conditions as defined in the DNV Classification Notes 30.8, namely the symmetric bottom slamming, the transverse split force, and the torsional/pitch-connecting moment load condition. These load conditions are assumed to be the most critical. From the finite element analyses, it is seen that the structural response for both models is quite similar.

Only the transverse split force load condition analyses showed stresses exceeding the allowable stress levels given in the DNV HSLC rules. However, the results indicated that the hull beam of the traditional model was slightly stiffer, so it is suggested that the plate thickness for the shell plating in the floating frame version is increased at some critical regions. An increase of the longitudinal stiffener shear area is also seen necessary to reduce high shear stresses at critical areas for the floating frame version.

A fatigue assessment of the longitudinal stiffener-transverse floating frame connection has been performed. Three different locations were identified as potentially critical in terms of excessive fatigue damage. Those were located at the middle of the stiffener flange at the weld toe, at the edge of the stiffener flange at the weld toe, and at the edge of the frame bottom flange. The long term distribution of stresses was approximated by a two-parameter Weibull distribution. The shape factor was set to 0.81 and the number of load cycles for 20 years of service was set to 100 million. The maximum stress range in the load history was assumed to occur for symmetric bottom slamming. Four finite element models of the structural detail were developed and analysed for determination of the maximum stress range. It was found by Miner summation that none of the locations considered would experience a critical fatigue failure for 20 years of service.

Preface

This thesis is written as the last step to complete my Master of Science in Marine Technology at Norwegian University of Science and Technology. It is a continuation of the project work performed by myself during the fall semester 2011 and the Master's Thesis' written by Jon Englund at KTH in december 2009 and Toralf Ervik at NTNU in june 2010.

Finite element modelling and analyses of those proved very time consuming, partly due to technical problems and my own lacking experience. In order to obtain satisfying results, some trial and error has been needed, but in the end I am satified with the results from the finite element analyses. This has lead to that some parts of the scope are left unanswerred, like the non-linear analysis of the longitudinal stiffener-floating frame connection. On the other hand, a slamming analysis has been performed, although it was not included in the scope. However, it was seen necessary to analyse in relation to the fatigue analysis, and also to compare the structural response of the strengthened floating frame with the floating frame as used in Toralf Erviks finite element models.

The cumulative fatigue damage was supposed to be calculated by both the nominal stress range approach and the hot spot stress range approach. The latter proved very difficult, as the hot spot stress range approach was designed for offshore steel structures. Consequently, no relevant SN-curves corresponding to the structural detail analysed were obtained. A possibility was to create my own SN-curve based on a series of assumptions to be used with the hot spot stresses, but this was thought to give very inaccurate results. A calculation of cumulative fatigue damange using the hot spot stress range approach was thus omitted from the thesis. As only nominal stresses were considered, there was no point in including a discussion about the stress concentration factors.

I would like to thank my supervisor Professor Jørge Amdahl at the Department of Marine Technology at NTNU for his invaluable guidance and help related to all aspects of this thesis. I would also like to express my gratitude to PhD Candidate Arswendy Arswendy (NTNU) for useful help related to finite element modelling, Norwegian Sportsperson of the Year 1970 Professor Stig Berge (NTNU) for providing relevant papers on fatigue, and Stig Oma at Fjellstrand AS for valuable comments related to technical aspects.

Trondheim, June 2011

Contents

List of Figures

List of Tables

Nomenclature

Symbols

a_{cg}	Design vertical acceleration at LCG
a_v	Design vertical acceleration
$a*$	Number of stiffeners between consideres section and nearest support
$\bar{a}$	Geometrical/material parameter in SN-curve
b	Distance between hull centerlines
$b*$	Breadth of load area
f_1	Mechanical property factor
g_0	Standard acceleration of gravity
h_0	Vertical distance from the waterline to the load point
k_a, k_b	Coefficients depending on element considered
k_l	Longitudinal slamming pressure distribution factor
k_r	Correction factor for curved plates
k_s	Sea load distribution factor
k_{sf}	Shear force factor
l	Stiffener span
m	See $\bar{a}$
$m*$	Bending moment factor
n	Number of hulls
n_0	Total number of load cycles in the load history
n_i	Number of cycles in stress range block i
p_{car}	Design pressure at car deck
p_{HS}	Hydrostatic pressure
p_{sp}	Design sea pressure
$p_{sp,keel}$	Design sea pressure at keel
$p_{sp,WL}$	Design sea pressure at waterline
$r*$	Average point load from stiffeners between considered section and nearest support
s	Stiffener spacing
t	Thickness
y_b	Distance from the center line to local center of one hull
z	Height from base line to NA of cross structure
A	Design load area
A_S	Minimum shear area for stiffener
A_W	Effective web area of girders
B	Beam over all
B_{hull}	Breadth of one hull
B_{MAX}	Maximum width of submerged part

B_{WL}	Maximum width in the water line
C_W	Wave coefficient
D	Cumulative fatigue damage
D_i	Fatigue for stress range block i
F_y	Horizontal split force on immersed hull
H	Stowage height
H_1	Maximum significant wave height in which the vessel is allowed to operate
H_S	Significant waveheight
L	Length of the craft
L_{BMAX}	Length where $B_{MAX}/B_{WL} > 1$
M	Bending moment
M_P	Twin hull pitch connecting moment
M_S	Twin hull transverse bending moment
M_{split}	See M_{TW}
M_{S0}	Still water transverse bending moment
M_t	Twin hull torsional moment
M_{TW}	Dynamic transverse bending moment
N_i	Number of cycle to failure for stress range block i
$P_{sl,b}$	Design bottom slamming pressure
$P_{sl,p}$	Design pitching slamming pressure
S	Stress range
S_0	Maximum stress range in the load history
S_G	Girder span
S_i	Applied stress range in block i
T	Fully loaded draught
T_0	Draught at L/2 at normal operation
T_L	Lowest service speed draught at FP
T_z	Zero crossing period
V	Maximum speed
Z	Section modulus
β_x	Deadrise angle at transverse section
β_{cg}	Deadrise angle at LCG
θ	Heading
λ	Weibull scale parameter
ξ	Weibull shape parameter
ξ_{WC}	Weibull shape parameter, worst case
ρ	Density of liquid
σ	Bending stress
σ_a	Stress amplitude
σ_e	Equivalent stress, Mises stress
σ_{sl}	Allowable bending stress for slamming load
σ_x	Bending stress in x-direction
σ_y	Bending stress in y-direction
τ	Shear stress
τ_{sl}	Allowable shear stress for slamming load
τ_{xy}	Shear stress in the xy-plane
ω	Wave frequency
ω_e	Wave encounter frequency
Δ	Fully loaded displacement

Abbrevations

CN 30.8	Classification Notes No. 30.8
DNV	Det norske Veritas
DOF	Degree of freedom
FEA	Finite element analysis
FP	Forward perpendicual
HAZ	Heat affected zone
HSLC	High speed, light craft and naval surface craft
JC60	JumboCat 60
LCG	Longitudinal center of gravity
LLC2	Local load condition 2
GLC4	Global load condition 4
GLC5	Global load condition 5
NA	Neutral axis
WL	Waterline

Chapter 1

Introduction

1.1 Scope

Konstruksjonsstyrke til bruksbåter og hurtiggående båter med prefabrikerte, utenpåliggende paneler i aluminium

Structural strength of work boats and high speed crafts with pre-fabricated, floating panels in aluminium

Aluminium er et hyppig brukt materiale for bygging av bruksbåter til oppdrettsnæringen, hurtiggående passasjerbåter og katamaranferger. Produksjon av båtskrog har tradisjonelt krevd mye arbeidsinnsats, med tilpassing av plater, stivere, spant og andre elementer, og et stort omfang av manuell sveising.

I prosjektet ALUBÅT er målsettingen å komme fram til mer kostnadseffektive måter for å produsere aluminiumsskrog til bruksbåter. Det er utviklet konstruksjonsløsninger og bygget mindre båter med utstrakt bruk av prefabrikkerte paneler, bestående av friksjonssveiste ekstruderte aluminiumsprofiler. Panelene er brukt til båtdekk, -sider og -bunn. Med paneler menes her hudplater med ferdige stivere.

En effektiv og økonomisk bruk av panelene i båtbygging forutsetter at panelene kan legges utenpå skott og tverrammer (spant). Dette til forskjell fra tradisjonell bygging av stål- og aluminiumbåter, hvor stivere påsveises platene. Videre føres stiverne normalt gjennom spantene via utsparinger i disse. Stiverstegene sveises normalt til spantene, men det er også eksempler på at de kun sveiste mot spantene i stiverens toppflens, evt. i kombinasjon med brakett for skjæroverføring.

Bruk av prefabrikkerte paneler bestående av ekstruderte profiler sammenføyd med friksjonssveis innfører ingen nye materialkvaliteter i båtbygging. Materialet som brukes er vanligvis aluminiumlegeringene 6082 og 6005A, i behandling T6, som har godt dokumenterte fasthetsegenskaper. Materialet svekkes ved sveising, men ikke vesensforskjellig fra andre vanlige brukte aluminiumslegeringer og leveringstilstander.

Skrogkonstruksjon med bruk av paneler hvor stiverne legges utenpå skott og tverrammer (spant) krever at det må regnes på mulig styrkereduksjon i kryssingspunktet mellom sti-

vere og skott/tverrammer. Beregningsanvisning for dette er ikke beskrevet i de vanlige dimensjoneringsregler for båter, hverken Nordisk Båtstandard av 1990 for yrkesbåter under 15 m eller Det norske Veritas regler for hurtiggående båter (High Speed, Light Craft and Naval Surface Crafts - HSLC). For hurtiggående båter aksepteres pr. dato ikke bruk av utenpåliggende paneler.

Det er derfor ansett nødvendig å utvikle modifiserte dimensjoneringsregler for prefabrikkerte paneler. En forutsetning har vært at de modifiserte regler skal ivareta sikkerhetsnivået som er implisitt i dagens regelverk.

Det var umiddelbart ikke klart hvilken dimensjoneringsfilosofi som ligger innbakt i Nordisk Båtstandards krav til platetykkelse og motstandsmoment for stivere. Tilsvarende krav i DnV's Tentative Rules for Certification and Classification of Boats, 1997 og DnV Rules for Classification of High Speed, Light Craft and Naval Surface Craft har derfor også blitt vurdert . Dette arbeidet har bidratt til å avdekke grunnlaget for kravene i Nordisk Båtstandard, og sammenligninger har vist at forskjellene mellom de tre regelverkene er moderate. Når det gjelder yrkesbåter under 15 m har man derfor valgt å foreta modifikasjon av Nordisk Båtstandard, som er den standarden aktuelle byggere av bruksbåter er kjent med. Det har her spesielt blitt sett på kravene til motstansmoment av stivere/spant utsatt for tverrbelastninger.

Styrkereduksjonen på grunn av opplagerkraft (konsentrert kraft) i kryssingspunkt mellom stivere og spant er tatt hensyn til ved at kravet til motstandsmoment økes proporsjonalt med den reduserende virkningen som forårsakes av den konsentrerte opplagerkraften. Det er tatt utgangspunkt i en anerkjent dimensjoneringsprosedyre for kapasitet for plater med konsentrert last på platerand gitt i Eurocode 9.

Et moment som kan ha betydning er evnen utenpåliggende paneler har til å oppta globale skjærkrefter via lastinnføring fra tverrspant. Denne overføringen kan kun skje via sveisen til panelets toppflens mot spant, i motsetning til over hele skipssiden ved tradisjonell utførelse. Globale skrogbelastninger har generelt mindre betydning for (små) bruksbåter og Nordisk Båtstandard inneholder derfor ikke krav til kontroll av global skjærkraft. HSLC har derimot et eksplisitt krav til en slik kontroll ikke minst da tverrspant kan bli utsatt for betydelige dynamiske laster ved høy fart i sjø.

Ved utenpåliggende panel vil ikke panelet bidra med effektiv flens til bøyning av tverrammene. Tverrammene må derfor dimensjoners for å bære lastene som innføres uten medvirking fra huden. Dette gir noe økte dimensjoner på tverrammene, men for øvrig synes det ikke å by på konstruktive utfordringer. Da tøyninger og spenninger i bunnen av tverrammene ikke overføres til huden, vil imidlertid huden få en relativ forskyving i forhold til bunnen av tverrammene. Det medfører en bøyning av stiverstegene i det prefabrikkerte panelet ut av stivestegets plan. I et tidligere arbeid utført av Jon Englund er disse spenningene funnet å være betydelige. Slike bøyespenninger er ikke til å unngå med utenpåliggende panel; spørsmålet er hvor store spenninger som kan aksepteres. HSLC reglene omhandler ikke direkte bruk av slike paneler og de spesielle tøynings- og spenningstilstander som opptrer ved bruk av panel-løsningene, slik at nye vurderinger må utføres.

Hensikten med denne oppgaven er å videreføre arbeidet til Jon Englund og Toralf Ervik. Den vil spesielt fokusere på spenninger fra globale laster; tverrskips bøyemoment, torsjonsmoment og "pitch-connecting" moment. Målet for oppgaven er å utarbeide grunnlag for å søke Veritas godkjennelse av en aktuell, planlagt hurtiggående båt fra Fjellstrand med

utenpåliggende paneler.

Oppgaven foreslås gjennomført i følgende trinn:

1. Beskrive relevante globale laster og styrkekrav for skrogbjelken i henhold til DnV HSLC. Gjennomgang av relevante anbefalte metoder for direkte styrkeberegninger gitt i DnV Classification Note No. 30.8.

2. Gjennomgang og forbedring av modell av skrogbjelken for Fjellstands 60M Jumbocat, utviklet i prosjektarbeidet høsten 2010. På grunnlag av denne modellen utføre lineære analyser av skroget utsatt for tverrskips bøyemoment og torsjonsmoment. Spenningsnivåene vurderes i forhold til akseptkriterier gitt i DnV HSLC og Class. Note 30.8. Spenningskomponenter som eventuelt ikke dekkes av disse reglene kommenteres og diskuteres.

3. Vurdering av konstruksjonens godhet med hensyn på utmatting. Det er her aktuelt å studere sveiseforbindelsene mellom panelene og tverrammene i skrogbunn og i skipsside. En detaljert elementmodell lages for å bestemme relevante spenningskonsentrasjonsfaktorer. Aktuelle levetidskurver for sveiseforbindelsene kartlegges, for eksempel med utgangspunkt i Eurocode 9 for konstruksjoner i aluminium. Spenningskonsentrasjonsfaktorer gitt i regelverk sammenlignes med resultat fra egne beregninger.

4. På grunnlag av enkle vurderinger utarbeides anslag på langtidsfordelingen til spenningsviddene, for eksempel basert på to-parameter Weibullfordeling. Utmattingslevetiden til forbindelsene beregnes, og følsomhetsvurderinger foretas.

5. I den grad tiden tillater kan det også foretas analyser av forbindelsenes sammenbruddsstyrke ved hjelp av ulineær elementmetode (Abaqus).

6. Konklusjoner og forslag til videre arbeid.

Referanser:

Jon Englund: *Structural strength of work boats and high speed crafts with floating frames*, MSc Thesis KTH, Centre for Naval Architecture, Stockholm, December 2009.

Jon Englund: *Oppsummering av FE-analyser på Jumbocat 60 med flytande ramar*, Oma 17.11.2009

Jon Englund: *Finit element-analys av Knut-Johan*, Oma 17.11.2009

Toral Ervik: *Structural strength of work boats and high speed crafts ith pre-fabricated, floating panels in aluminium*, MSc Thesis NTNU, June 2010.

Literature studies of specific topics relevant to the thesis work may be included.

The work scope may prove to be larger than initially anticipated. Subject to approval from the supervisors, topics may be deleted from the list above or reduced in extent.

In the thesis the candidate shall present his personal contribution to the resolution of problems within the scope of the thesis work.

Theories and conclusions should be based on mathematical derivations and/or logic reasoning identifying the various steps in the deduction.

The candidate should utilise the existing possibilities for obtaining relevant literature.

Thesis format
The thesis should be organised in a rational manner to give a clear exposition of results, assessments, and conclusions. The text should be brief and to the point, with a clear language. Telegraphic language should be avoided.

The thesis shall contain the following elements: A text defining the scope, preface, list of contents, summary, main body of thesis, conclusions with recommendations for further work, list of symbols and acronyms, references and (optional) appendices. All figures, tables and equations shall be numerated.

The supervisors may require that the candidate, in an early stage of the work, presents a written plan for the completion of the work. The plan should include a budget for the use of computer and laboratory resources which will be charged to the department. Overruns shall be reported to the supervisors.

The original contribution of the candidate and material taken from other sources shall be clearly defined. Work from other sources shall be properly referenced using an acknowledged referencing system.

The report shall be submitted in two copies:

- Signed by the candidate

- The text defining the scope included

- In bound volume(s)

- Drawing and/or computer prints which cannot be bound should be organised in a separate folder.

Thesis supervisor
Prof. Jørgen Amdahl

Contact person at Fjellstrand: Stig Oma

Deadline: June 15 2011

Trondheim, January 15, 2011

Jørgen Amdahl

1.2 Background

When designing a marine vessel, the designer tries to achieve minimum life cycle costs for the vessel while still fulfilling its requirements to serviceability and safety. For high speed, light craft and naval surface craft, there exists a wide range of rules addressing both serviceability and safety.

One of many important aspects of ship design is the weight of the hull. The payload will usualy be defined by the customer, so a challenge for the designer is to obtain minimum ship displacement while still fulfilling requirements set by both rules and customer. For high speed vessels, the hull resistance is often dominated by friction, as opposed to wave generation, which is the main contributor to hull resistance for most types of commercial ships. Thus, in order to minimize life cycle costs, hull weight is in general of more importance for high speed vessels than for other types of vessels.

While steel is the fabrication material for most commercial ships, high speed and light craft often use other, more lightweight materials. The mass density of aluminum is approximately one third of that of steel. Aluminum may be fabricated in practically the same way as steel, thus making aluminum an attractive fabrication material for the shipbuilders. There are however a few drawbacks concerned with the use of aluminum versus steel. Compared to steel, aluminum is more expensive, weaker, and has a significantly reduced fatigue performance [22].

Aluminum hull design has traditionally been very much alike the design of steel hulls. The hull girder strength in longitudinal and transverse direction has been provided by stiffeners, web frames, bulkheads, etc., all welded to the outer plating and decks of the vessel. The fabrication requires a lot of fitting and manual welding. It is desireable for the shipbuilders that the manual labour in the fabrication is kept to a minimum as it is generally less efficient and more expensive than automated fabrication.

The floating frame concept has been conceived as a measure to reduce both fabrication time and costs. This is achieved by significantly reducing the need for manual labour. As the concept name suggests, the transverse web frames of the vessel are floating, meaning that they are not welded to the outer plating as in traditional hull girder design. Instead, the web frames are placed directly on top of the longitudinal stiffeners, as illustrated in figure 1.1.
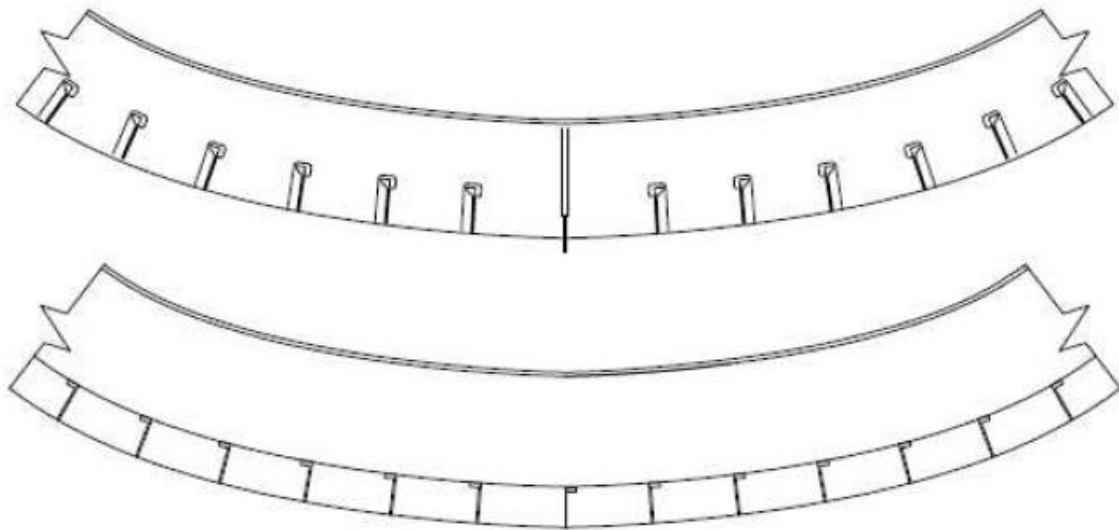
Figure 1.1: Above: Traditional hull girder design. Below: The floating frame principle.

The use of floating frames has up to now been limited to relatively small crafts, mainly work boats with lengths up to 15 meters. The seaworhiness of such crafts is not limited by the same set of rules that apply to larger vessels, i.e. rules set by classification societies. However, the trend of the latest years is that the displacement of work boats, for example used in the fish farming industry, has increased due to more advanced and heavier equipment installed on these work boats. The shipbuilders have complied to this industry demand by designing wider, not longer, work boats to avoid the need for classification as required for longer vessels.

Figure 1.2: Typical work boat used in the fish farming industry.

As of date, the rules set by the classification societies, for example Det norske Veritas (DNV), does not acknowledge the use of floating frames for vessels defined as High Speed, Light Craft and Naval Surface Craft, nor any other types of vessels. Prosjekt Alubåt was a research project launched and funded by the Norwegian Research Council with the purpose of aiding norwegian aluminum shipbuilders. Among the project participants were Norsk Industri, the Norwegian University of Science and Technology (NTNU), and several shipbuilders. One of the topics examined in the project was the use of floating frames for aluminum ships with lengths exceeding 15 meters. This would thus require a new set of rules or a modification of the current rules set by the classification societies. Prosjekt Alubåt ended in 2010 without any final conclusion in regards to the use of floating frames for larger aluminum vessels.

From a structural point of view, the floating frame concept is inferior to traditional hull girder design. By welding the tranverse web frames on top of the longitudinal stiffeners, the frames no longer have the outer plating acting as their bottom flange. This may be compensated for by adding a bottom flange to the transverse web frames and increasing the main dimensions. This will increase the hull weight as more material will be used to maintain the same strength as for the traditional design.

Another important issue is the distribution of stresses and possible stress concentrations. External forces acting on the outer plating can not be transfered directly from the outer plating to the transverse web frames, but must be transfered via the longitudinal stiffeners as bending and shear stresses. The weld in the stiffener-flange connection may potentially have to carry large loads. The strucure will be subjected to cyclic loading, so there may be some fatigue issues at the weld connecting the stiffeners and web frames. Large out-of-plane bending stresses in the stiffener webs may occur due to frame deflections.

(a) Floating frame

(b) Traditional frame
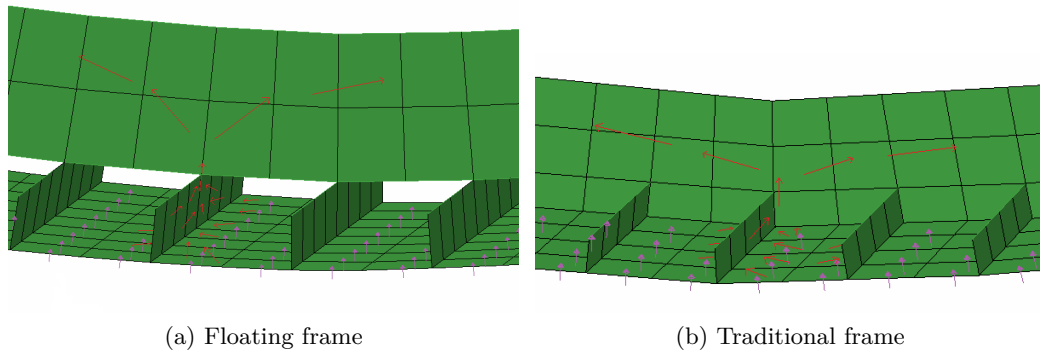
Figure 1.3: Distribution of external lateral pressure in bottom structure
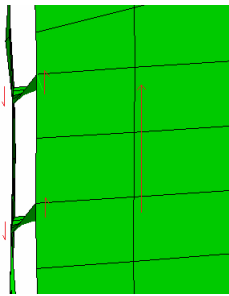
Figure 1.4: Out of plane bending of stiffeners at ship side, floating frame

1.3   JumboCat 60

The JumboCat 60 is a high speed catamaran introduced in 1996, and since produced various versions. It has a loading capacity of approximately 60 vehicles and 450-600 passengers.

Figure 1.5: The JumboCat 60

It has the following main dimensions:

- Length over all, LOA, 60.0 meters

- Length between perpendiculars, LPP, 54.0 meters

- Breadth, moulded, B, 16.5 meters

- Depth, moulded, D, 5.85 meters

- Draught, fully loaded, T, 2.24 meters

- Displacement, fully loaded, Δ, 580 metric tonnes

- Design speed, V, 35 knots

A norwegian yard has designed a modified version of the JumboCat 60 (JC60) with floating frames, and this design will be evaluated in the following sections. Specific details about the design will however not be included due to confidentiality reasons.

1.4 Previous work

1.4.1 JumboCat 60 with floating frames

As mentioned in 1.2, the possible use of floating frames was evaluated in Prosjekt Alubåt. Included in this evaluation were the Master's Thesis' written in 2009 and 2010 by Jon Englund at Kungliga Tekniska högskolan and Toralf Ervik at NTNU, respectively. Both Englund and Ervik performed finite element analyses (FEA) of a midship compartment of the JC60 with floating frames suscepted to what is defined as Local Load Condition 2, see section 2.2. Their analyses revealed structural stresses exceeding the allowable as defined by the strength requirements set by DNV, see section 2.3[12][11]. Ervik concluded that a strengthening of the transverse web frames was necessary to comply with the classification rules.

Furthermore, Ervik briefly discussed the fatigue performance of a selected structural detail, and found that it would have a fatigue lifetime exceeding the assumed 20 year lifetime of the vessel. The work of Englund and Ervik was continued by Lars Johan Mong. During the fall of 2010, he performed FEA for a simplified model of the JC60 with both traditional hull girder design and floating frames. At this point, the design of the floating frames were modified and a bottom flange was added to the transverse web frames. Subjected to a combination of torsional and pitch-connecting moment (see section 2.2), the models showed comparable strength, both within the requirements set by the rules [21].

1.4.2 The Floating Frame Principle

The floating frame principle has been used for various smaller vessels. The rescue crafts Knut Johan and at least four other rescue crafts of the Norwegian Rescue Company all had floating frames. Knut Johan had a length over all of 13.80 meters, a displacement of 20 metric tonnes, and a service speed of 20 knots. According to [1], Knut Johans floating frame section modulus was significantly lower than the required by Nordic Boat Standard. This was supported by Englund, who performed FEA on Knut Johan. He found that the bending stresses in the floating frames exceeded the allowable stress level [10]. Despite of this, an inspection of Knut Johan in 2006 discovered no structural deficiencies or weaknesses after 30 years of service [1]. This was also confirmed by the Norwegian Rescue Company and the Knut Johans crew.

Aalberg indicated that the interaction between the frame and the outer skin might be the reason why the structure proved strong enough. The conservativeness of the design loads was also deemed a possible explanation. The outer skin-floating frame interaction was evaluated by Ervik, and he showed that the outer plating and the longitudinal stiffeners provided only a small increase in stiffness as compared to the frame itself [12]. It should however be noted that Ervik studied the JC60 hull while Aalberg studied the hull of Knut Johan, two different hulls in terms of hull shape and frame design. The experience from Knut Johan can not be considered as completely compatible for other types of ships.

Latorre and Herrington of the University of New Orleans discussed the use of floating frames aluminum high-speed craft. They proposed a hull girder design with alternating fixed and floating transverse frames, and found that it had adequate strength for use in a 40 knot high speed craft with a length of approximately 40 meters [16]. This was confirmed by both FEA and experimental tests. It was also suggested that a proper selection of

panel components and available extrusions could provide a weight reduction of 15%. A continuation of the study was published in a paper in 2000. They confirmed the results, but did not provide any conclusions related to fatigue despite it being part of the study [17].

Chapter 2

Design loads and strength requirements

2.1 Design codes in general

A wide range of rules and regulations for seagoing vessels are intended to preserve the safety of life and goods. Three sets of rules with possible applicability for a large high speed vessel with floating frames has been evaluated in [2], namely

- Nordic Boat Standard,

- DNV Tentative Rules for Certification and Classification of Boats,

- DNV Rules for Classification of High Speed, Light Craft and Naval Surface Craft (DNV HSLC).

All of these sets of rules are intended for vessels with a traditional hull girder design. The use of them is hence problematic, and one needs to try to interpret the level of safety given by them implicitly to make them applicable for the case at hand. A combination of the three is impossible as the design loads are defined differently [2]. The most suitable and advanced set of rules has been identified as DNV HSLC, and will in the following be used as basis for determination of the structural integrity of the JC60 with floating frames.

2.2 Design Loads

The design loads to be considered are defined in DNV HSLC part 3, chapter 1. When considering the loads that will act on the vessel, no differentiation between traditional hull girder design and floating frame design is needed. In general, the loads are determined by the vessels main characteristics, service restriction, hull shape, etc. None of these factors differ when comparing traditional and floating frame design.

In the following sections, only those loads relevant for the load conditions to be examined are presented. They may be categorised as slamming loads, sea pressure, deck loads, transverse bending moments and loads, and pitch connecting and twin hull torsional moments.

2.2.1 Slamming Loads

[7] separates between bottom slamming and pitching slamming. They are defined, repectively, as

Sec. 2, C201 Bottom slamming

$$P_{sl,b} = 1.3k_l \left(\frac{\Delta}{nA}\right)^{0.3} T_O{}^{0.7} \left(\frac{50 - \beta_x}{50 - \beta_{cg}}\right) a_{cg} \tag{2.1}$$

Sec. 2, C203 Pitching slamming

$$P_{sl,p} = \frac{21}{tan(\beta_x)} k_a k_b C_W \left(1 - \frac{20T_L}{L}\right) \tag{2.2}$$

For frames, [12] found $P_{sl,b} = 82.3$ kN/m^2 and $P_{sl,p} = 80.7$ kN/m^2.

It is somewhat unclear how DNV arrived at these formulas, and it is difficult to determine the accuracy of the results. However it is assumed that the formulas provide conservative estimates of the actual slamming loads.

2.2.2 Sea Pressure

The sea pressure acting on the craft's bottom and side below design waterline is defined in Sec.2 C501 [7]:

$$p_{sp} = 10h_0 + \left(k_s - 1.5\frac{h_0}{T}\right) C_W \tag{2.3}$$

This gives $p_{keel} = 48.5$ kN/m^2 and $p_{WL} = 32.6$ kN/m^2. The values of the coefficients are taken from [18]. By comparison, the hydrostatic pressure at the keel, meaning at a depth of 2.24 meters, is $p_{HS} = 22.5$ kN/m^2.

2.2.3 Deck Loads

For the deck loads, it is convenient to distinguish between the car deck and the passenger deck. Section 2 C701 in [7] requires pressure on decks to be taken as:

$$p = \rho H (g_0 + 0.5a_v) \tag{2.4}$$

For accomodation decks, i.e. passenger decks, the load parameter is $\rho H = 0.35$ t/m^2, yielding a passenger deck pressure of $p_{pass} = 5.35$ kN/m^2 [18].

In [18], Økland investigated the difference of using point loads for the cars versus a distributed pressure over the area of the cardeck. He applied point loads of 15.3 kN for each wheel in one load case, and a distributed pressure of 4.0 kN/m^2 for the other load case. It was determined that the results from the two cases were practically identical. For simplicity, $p_{car} = 4.0$ kN/m^2 will thus be used.

2.2.4   Transverse Bending Moment and Split Force

[7] Sec.3 B202 states that the twin hull transverse bending moment shall be assumed to be the greater of:

$$M_S = M_{S0}\left(1 + \frac{a_{cg}}{g_0}\right) \tag{2.5}$$

$$M_S = M_{S0} + F_y(z - 0.5T) \tag{2.6}$$

In this case, where $a_{cg} = g_0$, this means the greater of double the still water transverse bending moment and the sum of the the still water transverse bending moment and moment induced by the transverse horizontal split force. The horizontal split force on the immersed hull is taken as:

$$F_y = 3.25\left(1 + 0.0172\frac{V}{\sqrt{L}}\right)L^{1.05}T^{1.30}(0.5B_{WL})^{0.146} \tag{2.7}$$

$$\cdot\left[1 - \frac{L_{BMAX}}{L} + \frac{L_{BMAX}}{L}\left(\frac{B_{MAX}}{B_{WL}}\right)^{2.10}\right]H_1 \tag{2.8}$$

However, Økland used a different formula, taken from an older version of the DNV HSLC rules:

$$F_y = 0.1L^2\left(1.6 - \frac{6}{\sqrt{L}}\right)\frac{70}{\left(\frac{L}{T}\right)^{1.5}}\left(1 + 0.1\frac{V}{\sqrt{L}}\right)\left(53 - \frac{L}{0.5B_{WL}}\right) \tag{2.9}$$

Obviously, there has been a modification of the formula. Økland also investigated the JC60. His version had a displacement of 560 metric tonnes and a draft of 2.15 meters. One would anticipate a smaller force for a vessel with lower draft and displacement given that the vessels were otherwise identical. This is however not the case. Using Øklands input data and equation 2.9, a horizontal split force of $F_y = 7204\,kN$ is found. Using the same input data and equation 2.8, we get $F_y = 1791\,kN$, about one quarter of the force found from equation 2.9.

The same goes for the case at hand. As expected, the force is slightly increased, giving $F_y = 7661\,kN$ from equation 2.9 and $F_y = 1889\,kN$ from equation 2.8. Heggelund, using the same input data as Økland, and referring to DNV HSLC rules, found the horizontal split force to be $F_y = 6304\,kN$. This value was also used by Økland in his analysis.

In Sec.3 B204, the still water transverse bending moment is given as

$$M_{S0} = 4.91\Delta\left(y_b - 0.4B^{0.88}\right) \tag{2.10}$$

This gives $M_{S0} = 4800\,kNm$. By simple integration, [15] derived another formula for determination of the still water transverse bending moment:

$$M_{S0} = \frac{\Delta gB}{8}\left(1 - 2\frac{B_{hull}}{B}\right) \tag{2.11}$$

This formula yields a still water transverse bending moment of $M_{S0} = 6472\,kNm$. It was however noted by Heggelund that equation 2.11 would yield conservative results as the weight of the pontoons and vessel sides increases the weight towards the sides of the vessel compared with the weight between the hulls.
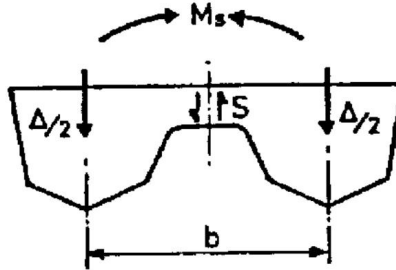

Figure 2.1: Still water transverse bending moment

For consistency, the formulas given in [7] will be used. Equations 2.5 and 2.6 yield $M_S = 9599$ kNm and $M_S = 13073$ kNm, respectively. The value z, denoting the distance from the baseline to the neutral axis for transverse bending, was set equal to 5.5 meters as in [15].

The latter article reveals some of the changes that has been made to DNV HSLC. The dynamic part of the transverse bending moment, i.e. the moment induced by the horizontal split force is given as $M_{TW} = F_y(z - 0.75T)$ as opposed to $M_{TW} = F_y(z - 0.5T)$ in equation 2.6. Consequently, the net horizontal split force has its centre of attack at 75% of the draught for the old formula and at 50% for the new formula.

However, this increase in distance from neutral axis does not compensate for the reduction of the horizontal split force. The dynamic transverse bending moment, M_{TW}, is found to have a value of 24552 kNm by Heggelund, while the current rules give a value of 8273 kNm.

Heggelund used VERES to determine the long term distribution of the transverse bending moment. Using linear calculations and a uniform distribution of wave directions, he found that for a probability of exceedence equal to 10^{-8}, the dynamic transverse bending moment had a value of about 4500 kNm given a maximum allowable significant wave height of 2.5 meters. The maximum allowable significant wave height is calculated from a formula given in section 2, B204, and has a value of 2.23 meters.

This indicates that conservatism is still preserved in the estimations of the design loads despite a dramatic change in the rules.

2.2.5   Pitch connecting and twin hull torsional moment

The twin hull pitch connecting moment is given in section 3, B301 as

$$M_P = \frac{a_{cg}L\Delta}{8} \tag{2.12}$$

Likewise, the twin hull torsional moment in section 3, B401, may be assumed to be
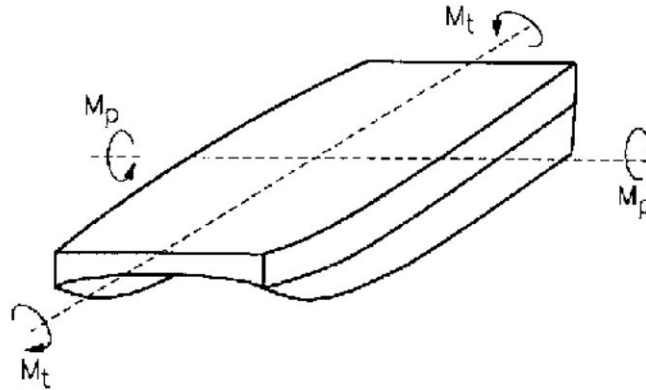
$$M_t = \frac{a_{cg}b\Delta}{4} \tag{2.13}$$

Figure 2.2: Combined torsional and pitch connecting twin hull moments

The pitch connecting and torsion moment was found to be, respectively, $M_P = 38406$ kNm and $M_t = 18207$ kNm. Heggelunds VERES analysis found, as mentioned in section 2.2.4, with a probability of exceedence of 10^{-8}, a torsional moment of about 4000 kNm given a maximum allowable wave height of 2.5 meters. One has to account for nonlinearities and other uncertaintis, but it is assumed that the calculated load is conservative in the present case.

2.3 Strength requirements

The strenght requirements are taken as defined in DNV HSLC Part 3, Chapter 3 - Hull structural design, aluminum alloy. These rules include requirements to manufacturing, member dimensions, allowable stresses, etc. In terms of allowable stresses, these are to be found using the design loads as defined in section 2.2. Those requirements relevant to the present case are presented in the following sections.

2.3.1 Hull girder strength

The rules regarding hull girder strength, both longitudinal and transverse, are given in section 4. A103 states that *"For new designs (prototypes) of large and structurally compli-cated craft (e.g. multi-hull types) a complete 3-dimensional global analysis of the transverse strength, in combination with longitudinal stresses, is to be carried out"*.

The hull section modulus requirement is given in B101:

$$Z = \frac{M}{\sigma} \tag{2.14}$$

The shear strength of the hull girder is to be sufficient so that the shear stress does not exceed, as given in C103

$$\tau = \frac{allowable\ bending\ stress}{\sqrt{3}} \tag{2.15}$$

It is to be evaluated for locations with doubtful shear area, which might be the case for the stiffener-frame interaction for the floating frame design.

For twin hulls, the connecting structure between the hulls is to have adequate transverse strength when subjected to transverse forces and moments as given in section 2.2. E201 defines the equivalent stress as

$$\sigma_e = \sqrt{\sigma_x^2 + \sigma_y^2 - \sigma_x\sigma_y + 3\tau_{xy}^2} \tag{2.16}$$

This is also known as the von Mises-stress. The allowable stresses, from E202, in the connecting structure are to be taken as:

Bending stress, σ $= 160\,f_1$
Shear stress, τ $= 90\,f_1$
Bending stress, σ_e $= 180\,f_1$

2.3.2 Plating and Stiffeners

Requirements to plating and stiffeners are defined in DNV HSLC part 3, chapter 3, section 5.

Maximum allowable bending stresses in plates and stiffeners, as in A301, are given in table 2.1.

Allowable bending stresses		
Item	Plate	Stiffener
	N/mm^2	
Bottom, slamming load	$200\,f_1$	$180\,f_1$
Bottom, sea load	$180\,f_1$	$160\,f_1$
Side	$180\,f_1$	$160\,f_1$
Deck	$180\,f_1$	$160\,f_1$
Flat cross structure, slamming load	$200\,f_1$	$180\,f_1$
Flat cross structure, sea load	$180\,f_1$	$160\,f_1$
Bulkhead, collision	$180\,f_1$	$160\,f_1$
Bulkhead, watertight	$220\,f_1$	$200\,f_1$

Table 2.1: Allowable bending stresses for plating and stiffeners

The thickness of the bottom plating is to be at least (B302):

$$t = \frac{22.4 k_r s \sqrt{P_{sl}}}{\sqrt{\sigma_{sl}}} \tag{2.17}$$

By this formula, the thickness requirement is 5.74 millimeters for the traditional design. For the floating frame design, one has to discuss whether the bottom plating should be assumed to be a heat affected zone (HAZ). The bottom plating is to be extruded with

longitudinal stiffeners and the extruded parts may be welded together so that the HAZ are located in noncritical areas. However, the bottom plating may at some point require repairs by welding. It is thus nonconservative to assume the bottom plating without HAZ. The minimum thickness of the bottom plating for the floating frame is estimated to 6.41 millimeters. The design bottom plate thickness is 6 and 7 millimeters for the traditional design and the floating frame design, respectively, thus exceeding the requirements.

From C201, the required section modulus of longitudinals supporting the bottom plating

$$Z = \frac{m * l^2 s P_{sl}}{\sigma_{sl}} \tag{2.18}$$

This gives a minimum value of 27.7 cm^3 for the traditional design and 34.6 cm^3 for the floating frame design. The traditonal design has bulb-100 profiles in its bottom structure with a minimum section modulus of 30.1 cm^3. The floating frame has T110 profiles for its bottom structure longitudinals with a minimum section modulus of 36.3 cm^3.

The required shear area of longitudinals, also given in C201

$$A_S = \frac{6.7(l - s)s P_{sl}}{\tau_{sl}} \tag{2.19}$$

Equation 2.19 was evaluated by [12] and found unsuitable for the floating frame design. He proposed the following formula

$$A_S = \frac{6.7 l s P_{sl}}{\tau_{sl}} \tag{2.20}$$

The minimum shear areas were found to be 3.34 cm^2 and 5.46 cm^2 for the traditional design and floating frame design, respectively. The shear area is assumed to be equal to the cross sectional area of the web of the profile. This area is 4.5 cm^2 for the bulb-100 profile used in the traditional design and 5.0 cm^2 for the T110 profile used in the floating frame design. A design modification is thus necessary for the bottom stiffeners in the floating frame design in order to meet the requirements. This can be done by choosing a stiffener with a larger shear area or using another material in order to reduce the shear area requirement.

2.3.3 Web frames and girders

The required strength of web frames and girders is given in DNV HSLC pt3. ch.3 Sec. 6. The maximum allowable stresses is as given in A401:

Allowable stresses			
Item	Web frames and girders		
	Bending stress (N/mm^2)	Shear stress (N/mm^2)	Equivalent stress (N/mm^2)
Dynamic load	$180\,f_1$	$90\,f_1$	$200\,f_1$
Sea/static load	$160\,f_1$	$90\,f_1$	$180\,f_1$

Table 2.2: Allowable stresses for web frames and girders

B401 and B402 states that the required section modulus and effective web area for girders subjected to lateral pressure is not to be less than, respectively:

$$Z = \frac{mS_G^2 b^* p}{\sigma} \tag{2.21}$$

$$A_W = \frac{10\,(k_{st}Sb^*p - a^*r^*)}{\tau} \tag{2.22}$$

There is no distinction between the two designs in terms of requirements as the input data for equation 2.21 and 2.22 are the same. These are $Z_{min} = 365.62$ cm^3 and $A_W = 36.5$ cm^2, respectively. The shear areas as of design are 18 cm^2 and 21 cm^2 for traditional and floating frame design, respectively. The wide gap in requirement and actual value appears inexplainable, but it is assumed that the shear area for both designs are sufficient as the traditional design is DNV approved. The minimum section modulus' for the frames are 438.77 cm^3 for the traditional design and 561.10 cm^3 for the floating frame design, both larger than the minimum requirement.

2.4 Direct calculation methods

The direct calculation methods presented in this section are taken from DNV Classification Notes No. 30.8, Strength analysis of hull structures in high speed and light craft. They are compatible with the DNV HSLC rules [5].

CN 30.8 distinguishes between transverse web frame analyses and global strength analyses. Web frame analyses deals with the structural response for a transverse web frame, normally located midships in the middle of a compartment, suscepted to extreme local loads. Global strength analyses addresses the global structural response when the vessel is subject to extreme global wave loads and/or loading.

For web frame analysis, a 3-dimensional finite element analysis may be applied. [5] advises that the model covers the length of one compartment in the midship are from base line to upper deck, and extend from centre of one compartment to centre of the next compartment.

Furthermore, it suggests that plating, webs and flanges are modelled as separate elements to ensure accuracy, and that 3 elements should be used over the height of the web of the frame. Boundary conditions should be applied to best model the reality.

For global strength analysis, the finite element model should in general cover the complete ship. CN 30.8 underlines the importance of including the geometrical hull shape, transverse

bulkheads, decks, and any torsional boxes. In the case that simplified modelling is applied, the simplifications has to be clearly identified and discussed.

Size and type of elements should be chosen to ensure that the effects of bending, shear and torsion of the hull beam are accounted for. Using four noded elements, CN 30.8 suggests using maximum three elements per frame spacing and three elements per tier. For FEM in general, a length to breadth ratio exceeding 3 is not advised as 'long' elements tend to perform poorly.

CN 30.8 lists seven load conditions for the web frame analysis and seven load conditions for the global strength analysis. Only three load conditions will be presented in the following sections. They are local load condition 2 (LLC2) - symmetric bottom slamming, global load condition 4 (GLC4) - transverse split force, and global load condition 5 (GLC5) - torsion moment/pitch connecting momemt.

2.4.1 Symmetric bottom slamming

This load case may be decisive for the bottom structure, and investigates the effect of slamming impact pressure on one frame. The slamming impact pressure is taken as found in section 2.2.1. The design load area is to be taken as the frame spacing times the length of the frame between the upper turn of bilge. It is also advised that, for a 3-dimensional model, the slamming pressure is applied to one frame and sea pressure on the bottom panels of the other frames.
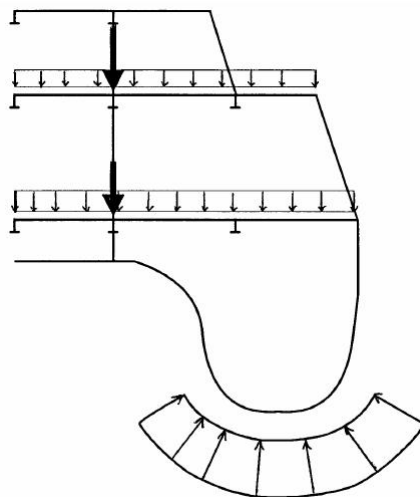

Figure 2.3: Local load condition 2, symmetric bottom slamming [5]

For the web frame analysis, e.g. the symmetric bottom slamming analysis, the acceptable stresses are taken as:

Design loads	Plating	Stiffeners and girders
Dynamic loads (slamming)		
- equivalent stress	220 f_1	200 f_1
- bending stress	200 f_1	180 f_1
Static loading (sea pressure)		
- equivalent stress	200 f_1	180 f_1
- bending stress	180 f_1	160 f_1

Table 2.3: Allowable stresses for web frame analysis

Allowable shear stress: $\tau = 90 f_1$

2.4.2 Transverse split force

The transverse split force load condition may be decisive for the structure between the hulls, the side and the bulkheads. The load case is meant to represent the maximum horizontal wave loads acting on the hull. This horizontal wave force is to be combined with the transverse still water bending moment. This load condition is in fact two different load cases, as one should consider both positive and negative split forces in combination with the still water transverse bending moment.
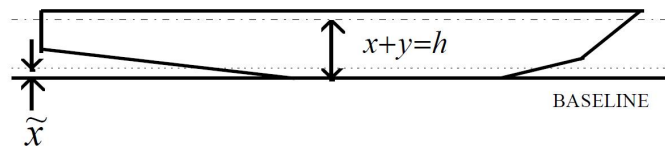
The transverse split bending moment in CN 30.8 is defined as

$$M_{split} = \frac{3}{4} F_y \cdot y + M_{s,keel} \tag{2.23}$$

$$M_{s,keel} = \frac{1}{4} \left[(x + y) - \tilde{x} \right] \tag{2.24}$$
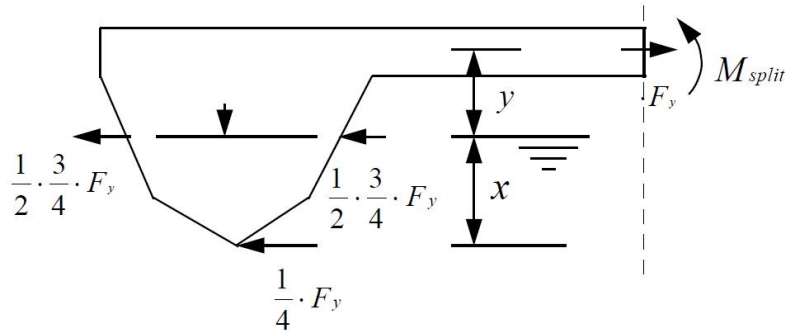
(a) Split load condition

(b) Geometrical definitions

Figure 2.4: Global load condition 4, transverse split force, split outwards shown

It is noted that *the sum of the horizontal forces is to act at 75% of the draught.* This is inconsistent with the rules, where $M_{split} = M_{TW} = F_y(z - 0.5T)$, as discussed in section 2.2.4. The is probably due to that CN 30.8 was published in August 1996, and is not been updated according to the current rules.

2.4.3 Torsion moment and pitch connecting moment

This load case combines the twin hull torsional and pitch connecting moment. It may be decisive for the cross structure. For the floating frame design, this load condition may cause large deflections of the frame relative the outer skin. This may induce high stresses in the longitudinal stiffeners.

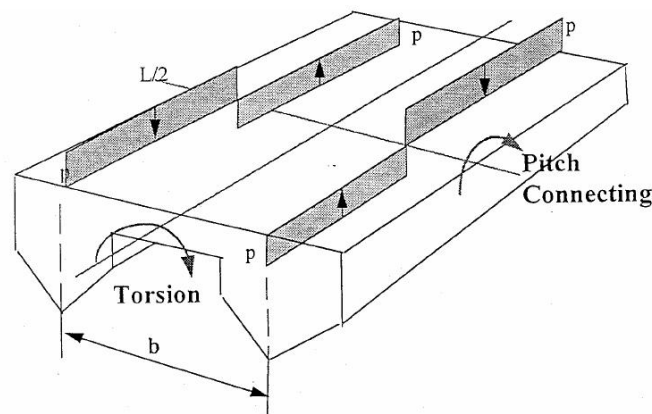As the figure shows, CN 30.8 suggests applying the moments as line loads in the deck of the model.

Figure 2.5: Possible modelling of global load condition 5, torsion moment/pitch connecting moment, [5]

Chapter 3

Finite Element Modelling

3.1 General

The finite element method is the common approach for structural analysis in general, and especially for marine structures as they are often complex structures and subject to a wide range of loads. Most structural problems are to complex to be solved by classical analytical methods, thus it is convenient to apply the finite element method to solve these problems. However, the results of a FEA are seldomly exact, but with experience and a correct interpretation of the results, the results will be accurate enough for engineering purposes.

The software used for the modelling was ABAQUS CAE, versions 6.9.2 and 6.10.2. The two versions are essentially the same in terms of functionality. ABAQUS standard has been used for processing the analyses, and ABAQUS viewer used for the post-processing.

The elements used are 4-node and 3-node thin shell elements and 2-node beam elements. As modelling is a time consuming task, the same meshes were used for all analyses. This is presented in more detail in sections 3.3 - 3.4. The models were built up by three different main parts:

- The outer plating and car deck, longitudinally stiffened, and the longitudinal bulkhead along the centerline. This part was extruded in the models length.

- The transverse web frames

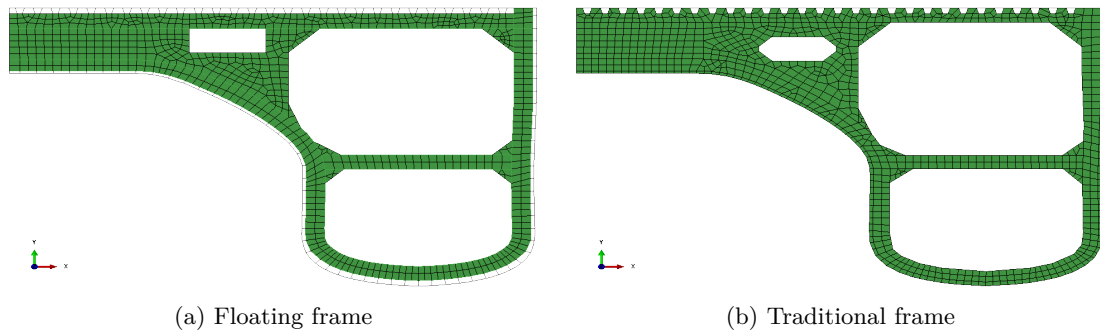- The transverse water tight bulkheads

(a) Floating frame

(b) Traditional frame

Figure 3.1: Web frames used in models

(a) Bulkhead, floating frame model
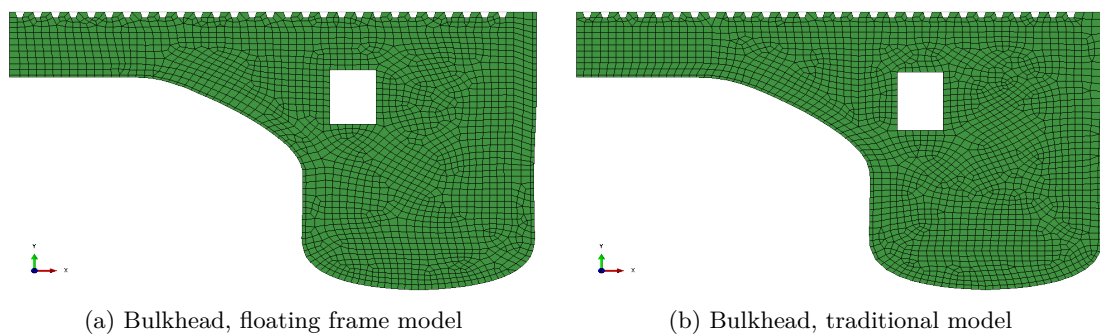
(b) Bulkhead, traditional model

Figure 3.2: Bulkheads used in models

As shown, no structural elements above the car deck were modelled. The upper decks and sides were neglected because it was assumed that the potentially critical structural response was to be found in the lower hull structure. However, the upper structure indeed contributes to some structural strength of the hull girder, thus implying that this simplification contributed to conservativeness in the analyses.

Some structural elements were neglected or simplified in cases where it was assumed that the simplification itself were of little importance for the present cases. Vertical stiffeners of the web frames and bulkheads were neglected as their main function is to prevent buckling. The same goes for the bracket flanges. These are however structural elements that would increase the structural strength, so the neglection of these element also contribute to conservativeness.

For all load cases, the same simplifications, loads, boundary conditions, etc., were practically equal for the floating frame model and the traditional hull girder model.
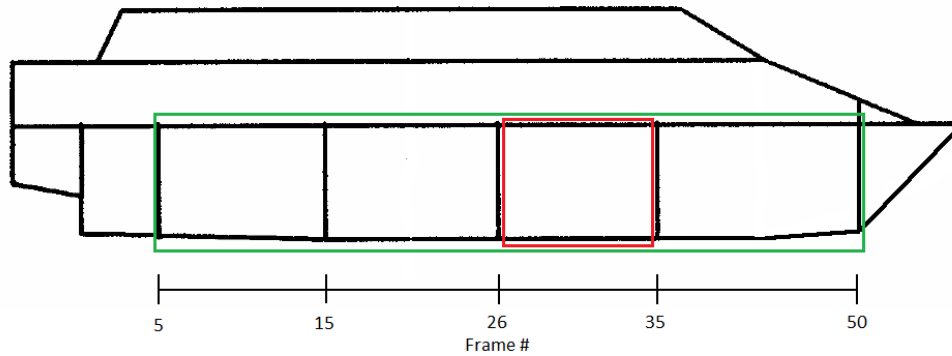
Figure 3.3: Extent of models, part highlighted in red used for the web frame analyses, part highlighted in green used for global analyses.

3.2 Torsion/pitch connecting model

The combined torsion/pitch connecting load condition is to represent the worst possible wave load in terms of torsion, meaning that the vessel is a moving through a wave that has a direction and wave period that gives the maximum torsional moment. In [14], Heggelund found that, given a forward speed of 35 knots, the extreme torsional moment occured for a wave direction of 66 degress (head sea = 0 degrees) and a wave period of 4.4 seconds.

The models used for the combined twin hull torsional and pitch connecting moment are simplified models of the complete vessels. The model length is 45 meters, stretching from frame #5 to #50 with a frame spacing of 1 meter, as specified in the drawings. The length over all of the vessel is 60 meters. In other words, the stern and bow of the vessel were not included in the model. This simplification was done to reduce the amount of work associated with the modelling. It was assumed that both weight and buoyancy contributions of the stern and bow was small, so the simplification should not represent a significant inaccuracy.
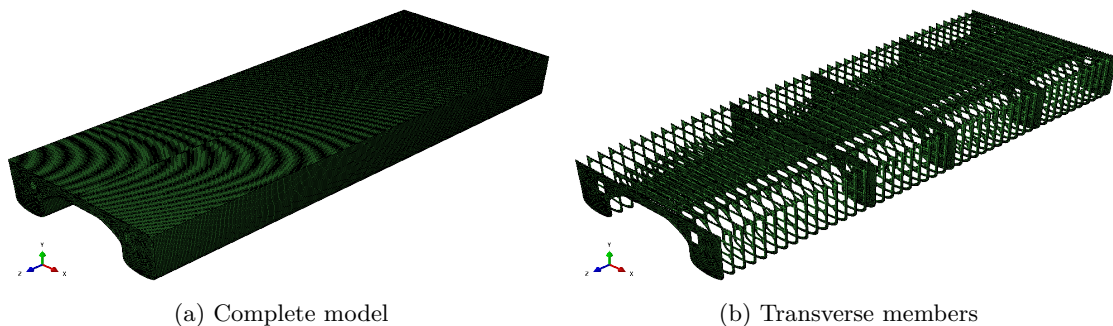

(a) Complete model   (b) Transverse members

Figure 3.4: Outlines of models used for torsion/pitch connecting analyses

Another simplification is the neglection of reduced cross sectional area towards the ends of the model. The transverse web frame at frame #27 and transverse bulkhead at frame

#26 located in the midship section of the vessel has been used to represent all web frames and bulkheads over the length of the model. Consequently, the cross section of the outer plating and car deck is constant over the length of the model. This implies a neglection of reinforcing structural elements and increased outer plating at the fore and aft sections of the vessel. It is however assumed that this modelling represents the hull girder strength in a satifactory fashion, and that the simplification itself is conservative.

As shown in section 2.4.3, it is suggested by DNV to apply the torsion and pitch connecting moment as constant line loads in the deck over the length of the model. In [14], Heggelund applied a linearly varying load between $-L/4$ and $L/4$ and constant otherwise. A better way to represent the actual load condition was assumed to be by applying the load to the immersed part of the hull. It also represented an oppurtunity to evaluate the stiffener-web frame interaction when the stiffeners were subjected to a lateral pressure.

For simplicity, the load was applied to the bottom structure, i.e. between the upper turns of the bilge, as an evenly distributed pressure. The net forces would thus act in the middle of the quarter-models. This is however inconsistent with DNVs proposal, where the net forces were to act in the middle of the quarter-vessels. By applying an evenly distributed pressure of 0.0192 N/mm^2 over the bottom structure and half length of the model, a pitch connecting moment of 38406.2 kNm was achieved, as estimated in section 2.2.5. However, this load yielded a twin hull torsional moment of 21848.8 kNm, 20% higher than the design load estimated by the rules. As discussed in section 2.2.5, the torsional moment is probably very conservative in the present case.

(a) Positive pressure   (b) Negative pressure
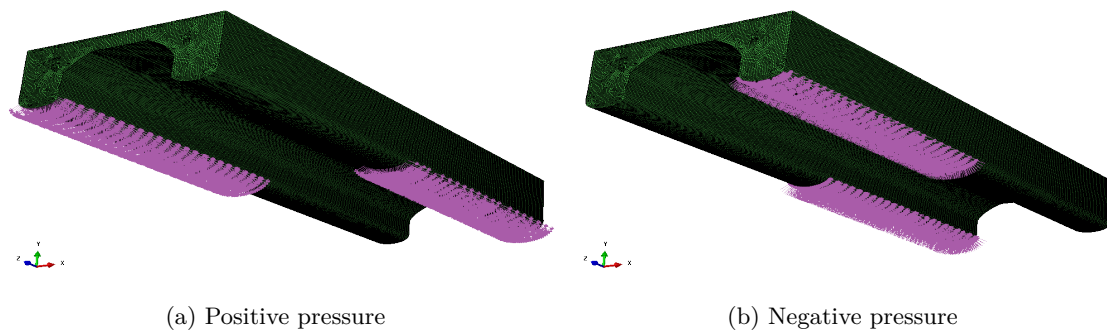
Figure 3.5: Idealised pressure distribution used in analyses

The sum of forces and moments acting on the models are zero, but boundary conditions were still needed to prevent rigid body movement that could be caused by minor defiencies in the modelling. The longitudinal axis is z, the transverse z, and the vertical y. The origin is located at the baseline, amidships at the centerline. By symmetry of forces, the model should be in balance at the centerline, midships, i.e. at x=0, z=0. However, fixing all degrees of freedom (DOFs) for all nodes at x=z=0 introduced numerical errors in the analyses. Two nodes at x=z=0 had all translational DOFs fixed, which surpressed potential rigid body translation and rigid body rotation about the z-, and y-axis. Springs counteracting longitudinal displacement were applied at the ship side. Their function was to prevent rigid body rotation about the vertical neutral axis.

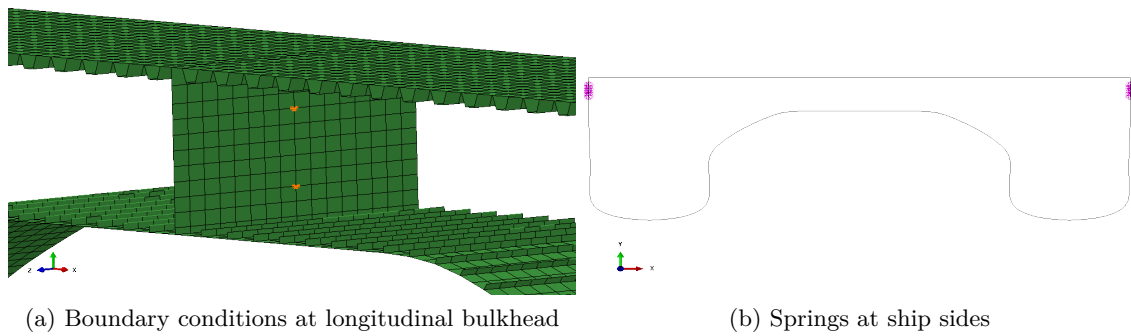(a) Boundary conditions at longitudinal bulkhead   (b) Springs at ship sides

Figure 3.6: Boundary conditions, torsion/pitch connecting moment

3.3   Transverse bending model

The models used for the transverse bending analysis are essentially the same models as used for the torsion/pitch connecting moment analysis, as explained in section 3.2. However, due to symmetry, only half the vessel was evaluated. The implications of the modelling simplifications are assumed to contribute to conservativeness and the models suitable to determine the structural response of the cross structure between the hulls and otherwise.

As prescribed by DNV, the split forces representing the horizontal wave forces are combined with the still water transverse bending moment. The still water transverse bending moment is applied as an evenly distributed pressure on the car deck, representing the weight of the vessel, and an evenly distributed pressure on the bottom outer plating, representing the vessels buoyancy. The values of these pressures are 5.7 kN/m^2 at the deck and 12.7 kN/m^2 at the bottom bilge, yielding a still water transverse bending moment of 4800 kNm about the neutral axis at $y = 5.5$ m, as estimated in section 2.2.4.

The splitforces were *not* applied as proposed in [5]. The reason for this, as discussed in section 2.2.4, was that there has been a rule change after the last version of DNV CN 30.8 was published. It was interpreted from [6] that the sum of horizontal forces were to act at 50% of the draught, not at 75% of the draught as suggested in DNV CN 30.8.

The split force was separated into three sets of concentrated forces. Two sets, being one quarter of the total split force each, were applied at both sides of the hull at the waterline. The last set, one half of the total split force, was applied at the keel point. Distributing the keel load and waterline loads over each node over the length of the models gave nodal concentrated forces of $F_{split,keel} = 2616.3$ N/node and $F_{split,WL} = 1308.2$ N/node. Positive and negative split forces were combined with the still water transverse bending moment in two separate analyses.

Symmetry was provided by fixing all nodes along the centerline (x=0) for all DOFs. This also prevented rigid body movement.
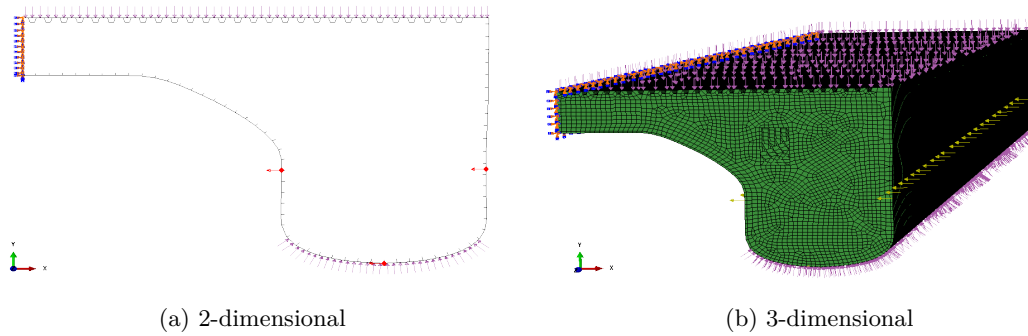
(a) 2-dimensional

(b) 3-dimensional

Figure 3.7: Loads and boundary conditions, transverse bending moment. Inward split force shown

3.4 Slamming model

The models used for the slamming analysis were similar to those used by Englund and Ervik for their slamming analyses. One half of the midship compartment from frame #26 to #35 was modelled. The models are consisted by the same three main parts as presented in section 3.1. As Ervik and Englunds analyses revealed structural stresses exceeding the acceptable levels as defined by DNV, it was desireable to perform the same analysis with the strengthened web frame compared to previous scantlings.

It is noted that both Englund and Ervik performed their slamming analysis with a more refined mesh than what is the case for this analysis. This should be taken into account when comparing the results, as a refined mesh normally indicates higher local stresses than a coarse mesh.

The meshes are in good compliance with the DNV CN 30.8 recommendations. Three elements over the web height of the frame should be used, the floating frame model has two and the traditional model has three. It is assumed that the meshes represents the true web frame structure in a satisfactory fashion.

The slamming load was applied to bottom plating between the the upper turns of the bilges in an area spaning longitudinally over a frame spacing. For the rest of the bottom structure, sea pressure was applied. The car deck pressure was applied as an evenly distributed pressure over the area of the car deck.

(a) 2D

(b) 3D, slamming load highlighted
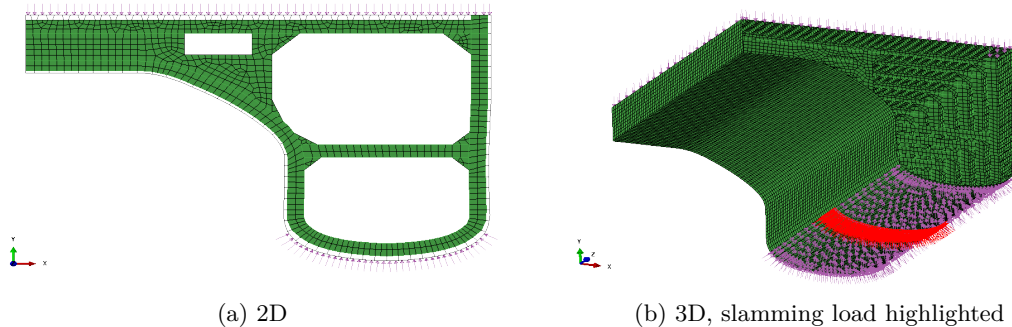
Figure 3.8: Pressure loads in slamming analyses

The force from the passenger deck for this particular half compartment is estimated to have a value of approximately 360 kN. It is assumed that about two thirds of this force is transferred through the ship side and the transverse vertical girder between the car deck and the passenger deck. The remaining third is carried by the centre pillars. For simplicity, this load is applied to the models at every web frame in the deck as distributed pressures over small areas, as shown in figure 3.9.

Figure 3.9: Modelling of passenger deck loads

The transverse bulkheads at the ends were not included in the model as the ends of the compartment had all DOFs surpressed. Also, a symmetry boundary condition was applied at the vertical plane along the centerline.

Figure 3.10: Boundary conditions in slamming analyses

Chapter 4
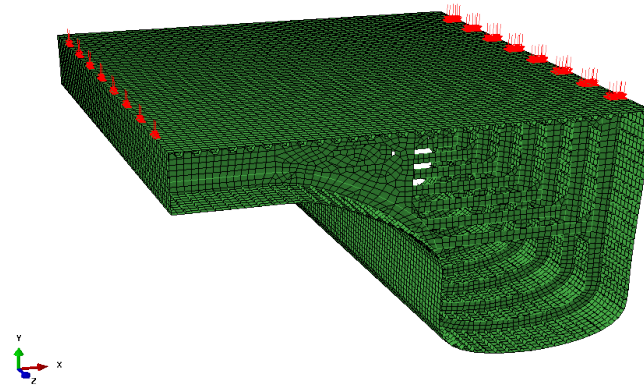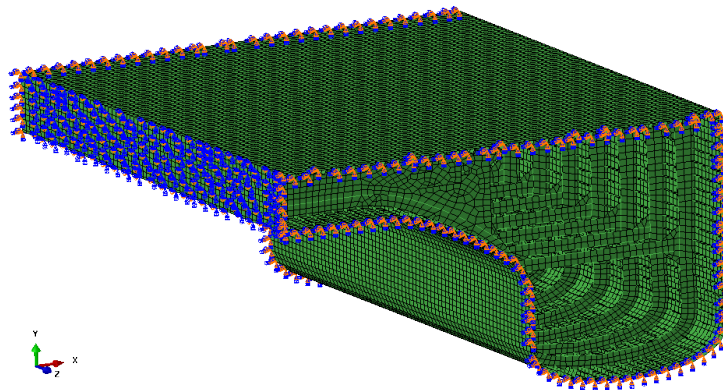
Results from finite element analyses

4.1 Interpretation of results

A finite element structural analysis is of limited value unless a correct interpretation and discussion of the results is undertaken. For complex structural problems, like the present cases, this is often a challenging task. Several sources of inaccuracy has to be considered, for example:

- Simplified geometry,

- simplified load modelling,

- poor element/mesh performance,

- numerical deficiencies,

- inaccurate boundary conditions

As discussed in chapter 3, the modelling is conservative, not only in a global sense, but also locally. For example, curved plates in the real structure are obviously modelled as a series of straight shell elements. As a consequence, the model surface is not as smooth as the real surface. This may affect the flow of stresses, possibly introducing stress concentrations that exceed the stresses in the real structure.

Stress concentrations may also be found where different structural members interact, e.g. longitudinal and transverse members. In the real structure, brackets, cutouts, flanges, etc., are applied to avoid high stress concentrations. Structural details like the above mentioned are not included in the models, and stress concentrations at certain locations should be expected and subsequently evaluated.

Deficiencies in the mesh may also introduce higher stresses for the models than what is the case for the real strucutre. Elements with poor element shapes or elements that are small compared to their surrounding elements, has a tendency of overestimating the stress level.

4.2   Torsion/pitch connecting analysis

The analyses with the complete model gave the results given in table 4.2. The corresponding allowable stresses are given in table 4.1.

Allowable stresses, global analyses, MPa		
	Plating and Stiffeners	Girders
Equivalent stress	86.4	108.0
Bending stress	76.8	96.0
Shear stress	43.2	54.0

Table 4.1: Allowable stresses, global analyses

Maximum stresses from torsion analyses, MPa				
	Floating frame		*Traditional*	
	Plating and stiffeners	Girders	Plating and stiffeners	Girders
Equivalent stress, S_{eq}	94.4	91.2	92.4	85.2
Bending stress, $|S_{11}|$	87.9	69.9	92.4	72.5
Bending stress, $|S_{22}|$	39.8	77.0	36.6	78.4
Shear stress, $|S_{12}|$	39.3	43.8	45.3	36.1
Ratio, maximum vs. allowable stresses				
Equivalent stress	109.3%	84.4%	106.9%	78.9%
Bending stress 1	114.5%	72.8%	120.3%	75.5%
Bending stress 2	51.8%	80.2%	47.7%	81.7%
Shear stresses	91.0%	81.1%	104.9%	66.9%

Table 4.2: Stresses from torsion analyses

The maximum stresses for the floating frame model are found to exceed the allowable. They are found at the longitudinal stiffeners flanges in the twin hull cross structure towards the ends of the model, at the intersection with frame #49.
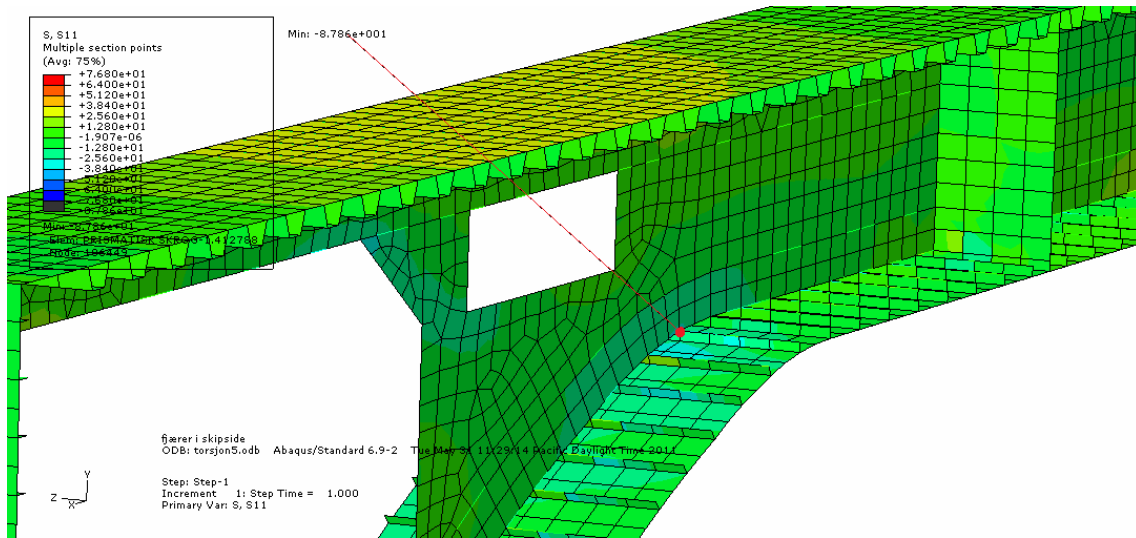
Figure 4.1: Bending stress at frame #49

Figure 4.1 shows the location of the maximum bending stress for the floating frame model. The stiffener flanges are modelled as beam elements, and ABAQUS viewer does not support rendered beam profiles for the contour plots. The location is thus manually highlighted with a red dot. The stress is concentrated in the flange, and high stresses are not found in the surrounding structure.

The equivalent stresses at the same location are shown in figure 4.2. Again, the maximum stress, as given in table 4.2, is located in the same stiffener flange, marked with a red dot. Stress concentrations are seen in the same region for the stiffener web and the plating. These stresses are however lower than the allowable stress.
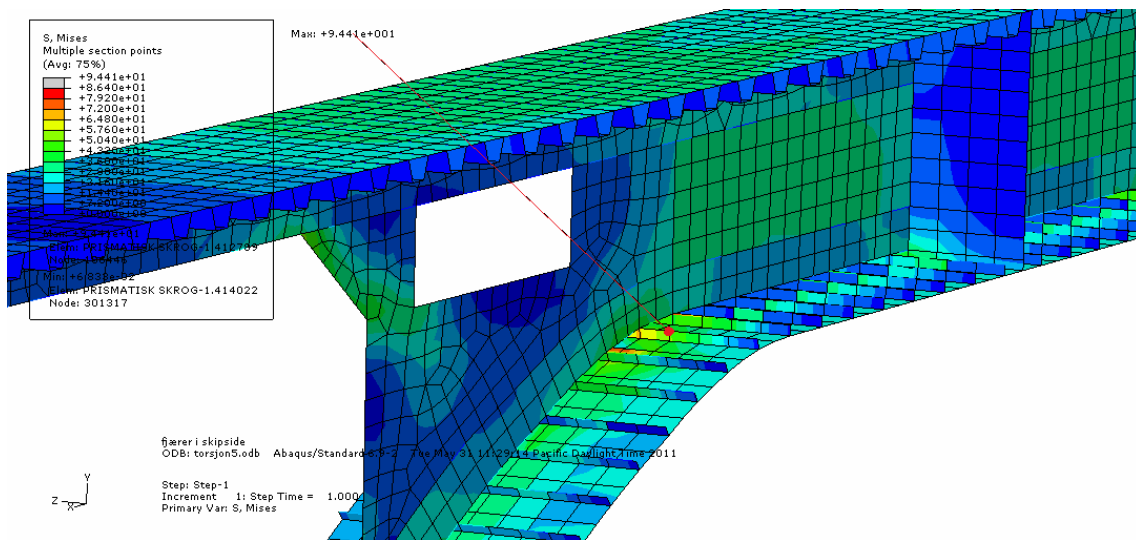

Figure 4.2: Equivalent stress at frame #49

By not considering the longitudinal stiffeners flanges, the maximum stresses in the floating frame model are within the allowable stresses. These stresses are found towards the ends of the model, at frame #5-6 and #49-50. The stresses closest to the allowable stresses are

found in the region as shown in figure 4.2. For the plating, equivalent and bending stress of about 90-95% of the allowable is found there. Also, the shear stress in the longitudinal stiffener web shown in figure 4.1 is 90% of the allowable.

The results of the traditional model are very similar to that of the floating frame model. The maximum equivalent and bending stress is found in a longitudinal stiffener flange in the twin hull cross structure at frame #15, at the intersection with a transverse bulkhead. As for the the floating frame model, the stress is local. Disregarding the longitudinal stiffener flanges, maximum equivalent and bending stresses for the traditional frame model are found to have values of about 86MPa and 80 MPa, respectively.

The models display slightly different torsional behaviour. Figure 4.3 shows a contour plot of the displacement magnitude for frame #50. It is seen that the displacements are slightly larger for the floating frame model, and that the torsional neutral axis is located higher for the traditional design than for the floating frame design.

(a) Floating frame   (b) Traditional design
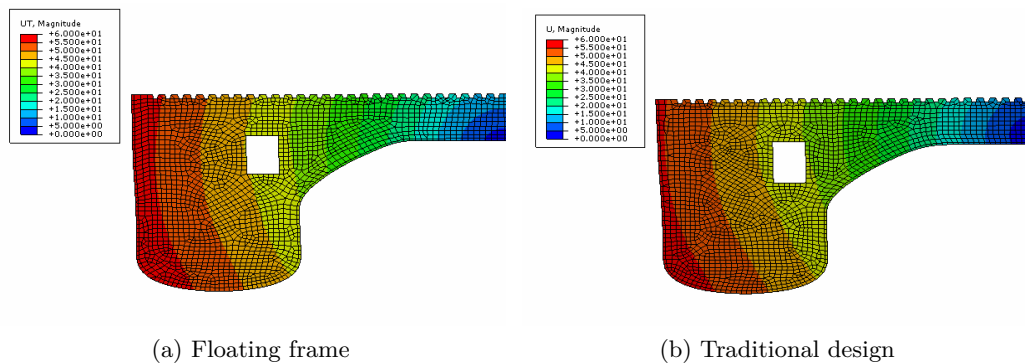
Figure 4.3: Comparison of torsional neutral axis

A simplified geometrical analysis of the torsional stiffness is summarized in table 4.3. Nodal displacements at the corner of the deck has been used for frame #50. Although the analysis being simple, it still serves as an indication of the torsional stiffness of the models. The displacements at the deck corner are larger for the floating frame model, and it is seen that this is partly due to a larger vertical distance between the torsional neutral axis and the deck for the floating frame model compared to the traditional model. The simple geometrical analysis yields torsional angles of 0.401 and 0.387 degrees for the the floating frame model and the traditional model, respectively.

Torsional deformation at deck corner, frame #50			
	Floating frame	*Traditional design*	*Unit*
Neutral axis height	4425.83	4726.24	mm
Height at deck corner	5850.00	5850.00	mm
Vertical distance above NA	1424.17	1123.76	mm
Horizontal distance from NA	8250.00	8250.00	mm
Undeformed angle, α_0	0.1709	0.1354	rad
	9.7943	7.7567	deg
Vertical disp. at corner	57.53	55.84	mm
Horizontal disp. at corner	-11.01	-6.95	mm
Deformed angle, α_1	0.1779	0.1421	rad
	10.1951	8.1439	deg
Torsional angle, $\phi = \alpha_1 - \alpha_0$	$7.00 \cdot 10^{-3}$	$6.75 \cdot 10^{-3}$	rad
	0.4008	0.3872	deg
Ratio, torsional rotation	103.53%	100.00%	

Table 4.3: Torsional stiffness

The combined pitch connecting and torsional moments induce warping deformations in the cross sectional planes. This effect is at its most predominant at the midsections of the vessel. Figure 4.4 shows combined undeformed/deformed contour plots of the longitudinal deformations at frame #27 for both models. The deformations are scaled 100:1.
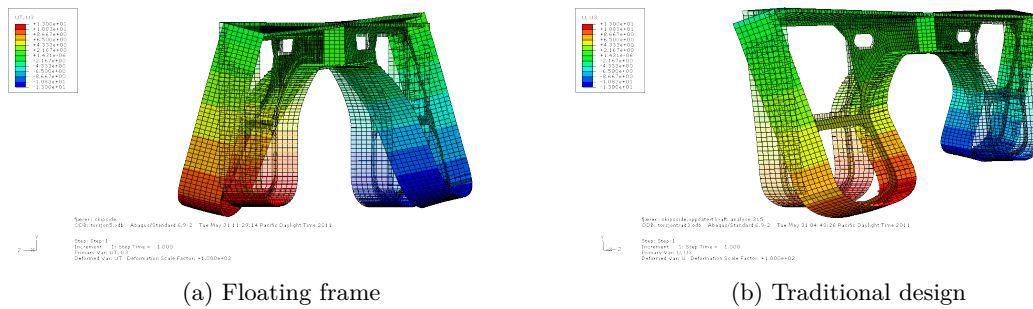

(a) Floating frame (b) Traditional design

Figure 4.4: Comparison of warping deformation at frame #27

The longitudinal warping deformations are found to have maximum values of about 12 and 13 millimeters for the traditional design and floating frame, respectively. Relatively large shear stresses are found in the plating in the same regions, 39.3 MPa for the floating frame model and 34.9 MPa for the traditional model.

4.3   Transverse bending analysis

The transverse bending load condition is considered as two separate load conditions. Both inward and outward split force is combined with the transverse still water bending moment. When considering the port half the vessel, the still water transverse bending moment is acting clockwise (looking from stern to bow) about the longitudinal neutral axis located at the centerline in the twin hull cross structure.

The inward splitforce gives a transverse bending moment acting counterclockwise abouth the neutral axis, thus counteracting the still water bending moment. This load condition is labeled transverse bending analysis 1, and the results from the analyses are listed in table 4.4.

Maximum stresses from tranverse bending analyses 1				
	Floating frame		*Traditional*	
	Plating and stiffeners	Girders	Plating and stiffeners	Girders
Equivalent stress, S_{eq}	49.1	41.7	53.6	44.9
Bending stress, $|S_{11}|$	47.1	36.9	52.7	41.3
Bending stress, $|S_{22}|$	18.8	28.8	19.0	33.6
Shear stress, $|S_{12}|$	25.3	20.3	29.2	21.1
Ratio, maximum vs. allowable stresses				
Equivalent stress	56.8%	38.6%	62.0%	41.6%
Bending stress 1	61.3%	38.4%	68.6%	43.0%
Bending stress 2	24.5%	30.0%	24.7%	35.0%
Shear stresses	58.6%	37.6%	67.6%	39.1%

Table 4.4: Allowable stresses and stresses from analyses

As expected, tranverse bending analysis 1 does not yield high stresses. The maximum stresses found are generally only 50-70% of the allowable for both analyses, and they are found to be slightly higher for the traditional model than for the floating frame model.

For transverse bending analysis 2, the horizontal split force is acting outwards, thus giving a clockwise transverse bending moment about the neutral axis. The maximum stresses are listed in table 4.5.

Maximum stresses from tranverse bending analyses 2				
	Floating frame		*Traditional*	
	Plating and stiffeners	Girders	Plating and stiffeners	Girders
Equivalent stress, S_{eq}	132.6	115.6	137.0	108.0
Bending stress, $|S_{11}|$	132.6	115.0	137.0	102.8
Bending stress, $|S_{22}|$	57.4	85.8	50.8	100.3
Shear stress, $|S_{12}|$	73.0	41.0	62.6	38.1
Ratio, maximum vs. allowable stresses				
Equivalent stress	153.5%	107.0%	158.6%	100.0%
Bending stress 1	172.7%	119.8%	178.4%	107.1%
Bending stress 2	74.7%	89.4%	66.1%	104.5%
Shear stresses	169.0%	75.9%	144.9%	70.6%

Table 4.5: Maximum stresses from analyses

Large stresses are found in both models. For the traditional model, all maximum stresses are found to exceed the allowable, implying that the models overpredict local stress concentrations, and that at least some of these may be neglected. The maximum bending, bending and shear stresses occur at region 1 at frame #35, as shown in figure 4.5. Extreme values are located in the longitudinal stiffener flange. Due to the simplified modelling of the stiffener flanges and their interactions with transverse bulkheads and transverse web frames, the stresses at these are expected to be highly overpredicted.
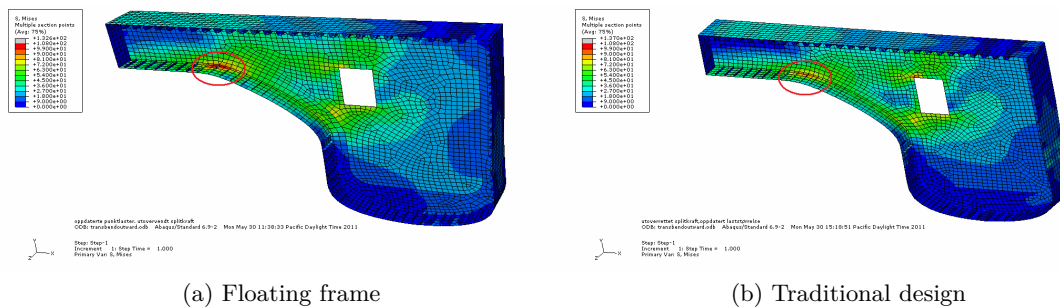

(a) Floating frame   (b) Traditional design

Figure 4.5: Equivalent stress at frame #35, region 1 highlighted

In figure 4.5, the stress range is such that dark red corresponds to 108 MPa, the maximum allowable equivalent stress for girders. It is seen that the stress level for the floating frame model is somewhat higher at region 1. For this load condition, the transverse bulkheads are carrying a significant part of the load as they are far stiffer than the transverse web frames. A higher stress level at the bulkheads for the floating frame model than for the

traditional model bulkheads may indicate that the traditional frames are carrying more of the load than the floating frames.

4.3.1   Transverse bulkheads

For the traditional model, the maximum equivalent and bending stresses found in region 1 for frames #5, #15, #26, #35 and #50 are in the vicinity of the allowable stress ranges. These stresses are however assumed to be somewhat overpredicted as the actual structure has a smoother turn than what is seen in the model. Also, the bottom elements in region 1 are quite small compared to the surrounding elements, thus making a overprediction of the stress probable.

The stress levels for the floating frame model are higher, and stress concentrations exceeding the allowable stress level are found at all bulkheads at region 1. The stresses are dominated by transverse bending stress, and the shear stress at region 1 is close to zero.

(a) Equivalent stress   (b) Transverse bending stress
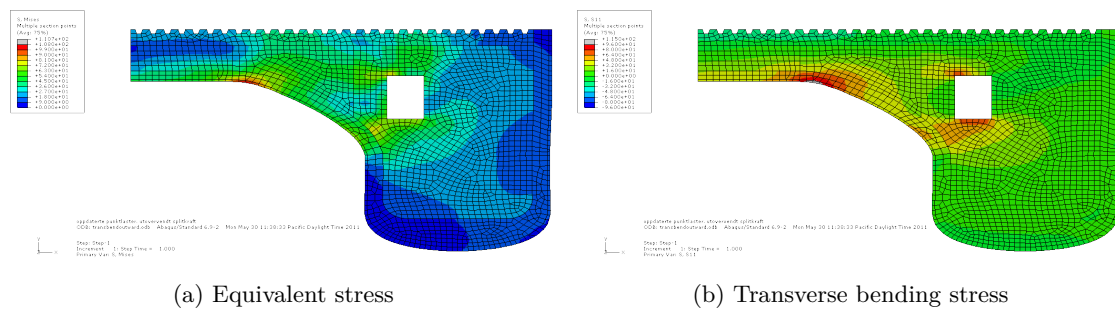
Figure 4.6: Stress at frame #35, floating frame model

For figures 4.6a and 4.6b, dark red colour corresponds to the maximum allowable stresses, 108 MPa and 96 MPa, respectively. Areas in light gray have stresses exceeding the allowable. These areas are expanded in figure 4.7. The maximum equivalent stress is 110.7 MPa, and the maximum bending stress is 115.0 MPa, 20% above the allowable bending stress.

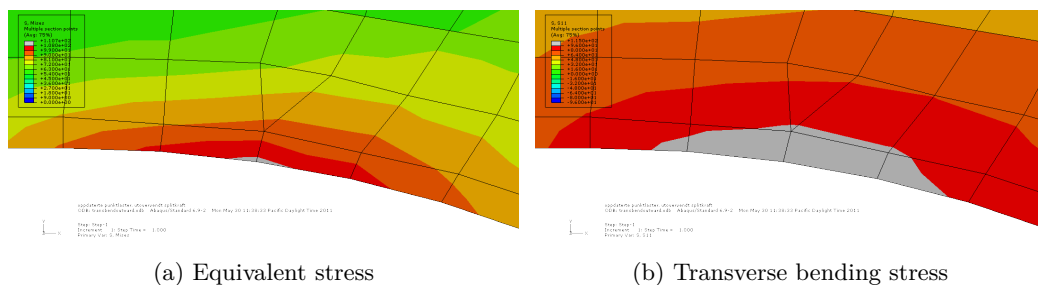(a) Equivalent stress   (b) Transverse bending stress

Figure 4.7: Extent of area with higher stress than allowable

The exceedance of maximum allowable bending stress extends over several elements, and may thus be critical for the structure. However, the modelling of the bulkheads is conservative, so an overprediction of the stresses is highly probable. If the bulkheads were to be strengthened, an increase of plate thickness in the areas around region 1 would probably be sufficient to reduce the bending stresses to an acceptable level.

4.3.2 Transverse web frames

In figure 4.8 dark red correspond to maximum allowable stress, while dark red and dark blue correspond to maximum allowable stress in figure 4.9. Higher stresses are found in the traditional frame than for the floating frame. This may indicate that the traditional frames carries more load than the floating frames for the present case. The maximum stresses found for the floating frame are about 80-90% of the allowable. For the traditional frame, a maximum equivalent stress of 107.9 MPa is found in region 2. This stress is dominated by the vertical bending stress at the same location, with a value of 100.3 MPa, 4.5% higher than the allowable stress. This stress concentration is however confined within one element.

The stress concentrations seen in region 2 are assumed to be overpredicted. Firstly, the models are simplified in the sense that rounded corners for the vessel are sharp corners in the model. Secondly, the relative difference in size of neighbouring elements is large.
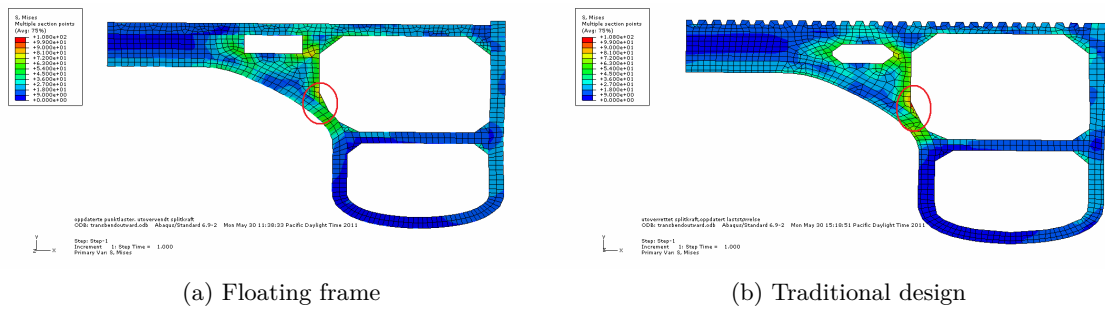

| (a) Floating frame | (b) Traditional design |

Figure 4.8: Equivalent stress at highest loaded transverse web frame, region 2 highlighted

| (a) Floating frame | (b) Traditional design |

Figure 4.9: Bending stress at highest loaded transverse web frame

4.3.3 Plating and stiffeners

Very high, local bending stresses were found in the longitudinal stiffener flanges. However, they are neglected in this section as the stress prediction for them is assumed to be exaggerated for the present case due to the modelling of the stiffener flanges. High stresses are also found in the plating and the stiffener webs.

For the plating, transverse bending stresses exceeding or close to the allowable level are found at region 1 for both models. Theses stress concentrations are located at frames #5,

#15, #26, #35, and #50, i.e. at all transverse bulkheads. As for the bulkheads, stress levels for the floating frame model are somewhat higher than for the traditional model. The maximum equivalent stress is 106.5 MPa at frame #35, about 14% higher than for the traditional model and 23% higher than the allowable equivalent stress at that location. The bulk of the equivalent stress is transverse bending stress, having a maximum value of 103.1 MPa at the same location. This is 25% higher than for the traditional model and 34% higher than the allowable bending stress.

Since also the traditional model also has equivalent stresses and bending stresses exceeding the allowable stress levels, it is reasonable to assume that the analyses has overpredicted the stresses in the plating, and that the actual plating stresses for the traditional model are within the allowable stress levels.

The increase of stresses for the floating frame model is primarily due to reduced stiffness in transverse bending compared to the traditional model. This yields larger global and local deformations. The largest local deformations are obviously found in region 1, at the transverse bulkheads. These local deformations are shown in figure 4.10, scaled 100:1. The contour plot displays rotational deformations.
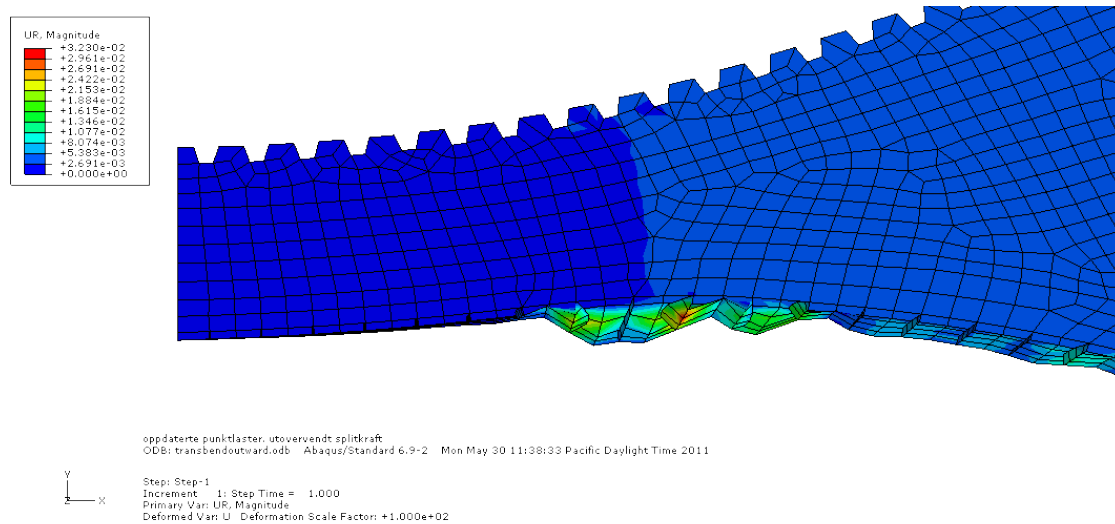

Figure 4.10: Local deformation at region 1, frame #35 floating frame model

A comparison of the plating equivalent and bending stresses at frame #35 for the two model are shown in figures 4.11 and 4.12. Areas where the stresses exceed the allowable stress level have light gray colour.
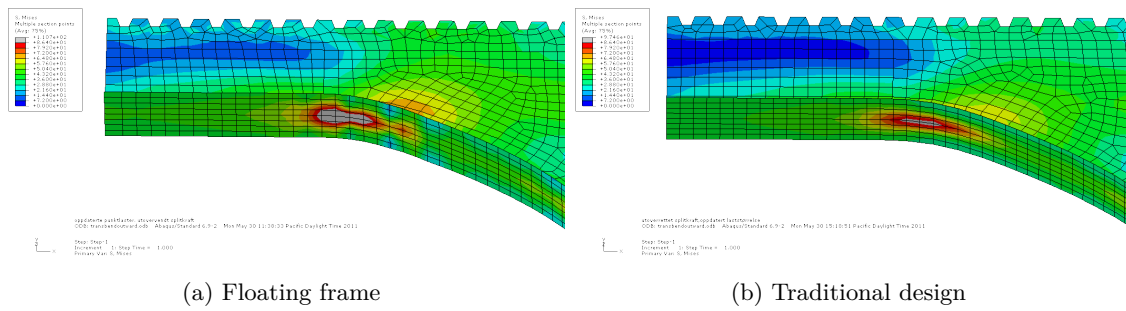
(a) Floating frame (b) Traditional design

Figure 4.11: Comparison of plating equivalent stress

It is seen that the area where the maximum allowable stress level is exceeded is quite large for the floating frame model. However, figure 4.12 reveals a rather untidy bending stress distribution for the floating frame model. This may indicate that there are errors in the modelling or in the finite element analysis itself, thus introducing inaccuracies in the results.

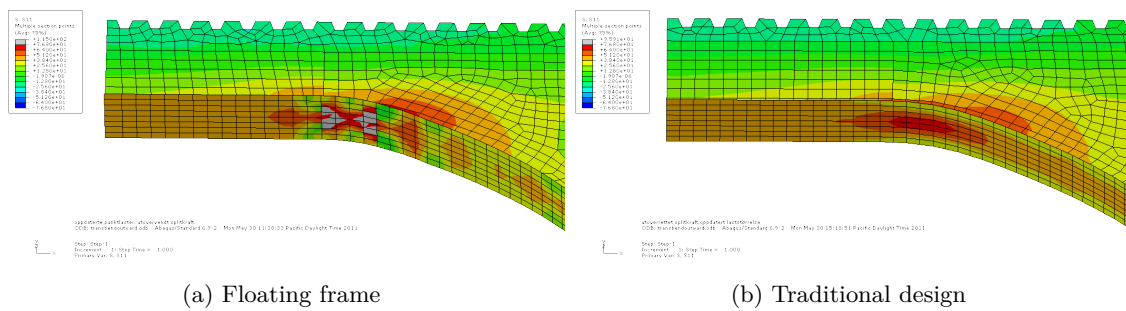
(a) Floating frame (b) Traditional design

Figure 4.12: Comparison of plating bending stress

In order to reduce the stresses in the plating structure for the floating frame model, the best solution is probably to increase the plating thickness at the critical areas. This is assumed to be sufficient as the stresses are dominated by transverse bending stress, and that other stress components are relatively small.

Stresses in the longitudinal stiffener webs are found to have values exceeding the allowable stress levels by wide margins. They occur at region 1, and are shear dominated. Due to the simplicity in the modelling of the stiffener-bulkhead interaction, stresses are exaggerated in the analyses. As for the bulkhead and the plating, the stresses from the floating frame analysis exceed those from the traditional design analysis. This is has two main explanations. Firstly, the local deformations, as shown in figure 4.10, are larger for the floating frame model. Secondly, the shear area of the T55-profiles used in the floating frame model at region 1 is 27% lower than for the bulb-65 profiles used in the traditional model.

The equivalent stress for the stiffener flange at region 1 has a maximum value of 128.6 MPa for the floating frame model and 115.2 MPa for the traditional model. These values are 49% and 33% higher than the allowable equivalent stress. Once again, this indicates that the stresses are highly overpredicted as the traditional design is DNV approved.

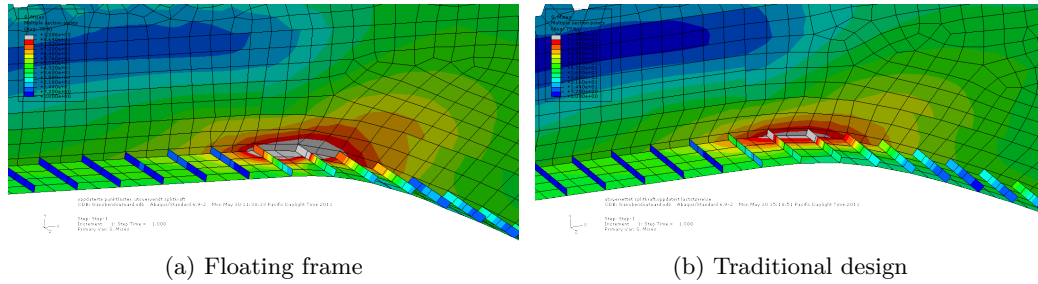(a) Floating frame   (b) Traditional design

Figure 4.13: Comparison of stiffener web equivalent stress, frame #35

In figure 4.13 and 4.14, the light gray areas indicate equivalent and shear stresses exceeding the allowable stress levels. The stiffener webs has maximum shear stress values of 73.0 MPa and 62.6 MPa for the floating frame model and the traditional model, respectively. They exceed the allowable shear stress by 69% and 45%.
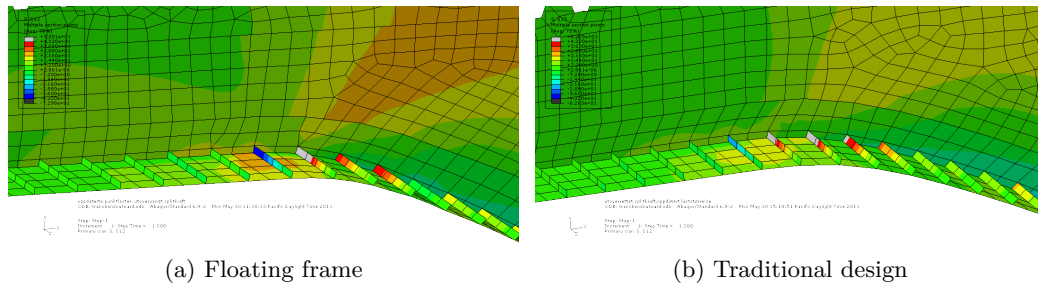

(a) Floating frame   (b) Traditional design

Figure 4.14: Comparison of stiffener web shear stress, frame #35

Although the modelling has been performed in a conservatice manner, it is probable that the longitudinal stiffeners for the floating frame design has stresses that are too high. To reduce the shear stress, and hence the equivalent stress, the stiffeners shear area needs to be increased. This implies that the height or the thickness of the stiffener webs needs to be increased, possibly both height and thickness. It should also be noted that a bulb-profile has better shear properties than a T-profile. A bulb-profile may however prove unsuitable for the floating frame design as the transverse web frame bottom flange is to be welded to the longitudinal stiffener flange.

4.4   Slamming analysis

The maximum stresses found in the slamming analysis are shown in table 4.7. The corresponding allowable stresses are shown in table 4.6.

Allowable stresses, web frame analysis, MPa			
	Plating	Stiffeners	Girders
Equivalent stress	105.6	96.0	120.0
Bending stress	96.9	86.4	108.0
Shear stress	43.2	43.2	54.0

Table 4.6: Allowable stresses, web frame analysis

Maximum stresses from slamming analysis, MPa						
	Floating frame			*Traditional design*		
	Plating	Stiffeners	Girders	Plating	Stiffeners	Girders
Equivalent stress, S_{eq}	39.3	65.6	57.2	40.5	67.8	78.0
Bending stress, $|S_{11}|$	36.9	65.6	57.2	41.2	67.8	72.8
Bending stress, $|S_{22}|$	36.9	18.6	52.9	36.5	25.0	86.5
Shear stress, $|S_{12}|$	22.4	16.7	22.5	23.0	24.7	24.4
Ratio, maximum vs. allowable stresses						
Equivalent stress	37.2%	68.3%	47.7%	38.4%	70.6%	65.0%
Bending stress 1	38.4%	75.9%	53.0%	42.9%	78.5%	67.4%
Bending stress 2	38.4%	21.5%	49.0%	38.0%	28.9%	80.1%
Shear stresses	51.9%	38.7%	41.7%	53.2%	57.2%	45.2%

Table 4.7: Maximum stresses from slamming analyses

It can be seen that all stresses found from the analyses, for floating frame and traditional design, are well within the strength requirements. The general tendency is that the stresses for the traditional design is slightly higher. By comparison, [18] found maximum stresses of about 90% of the allowable stresses in the bottom region of the web frame for the traditional frame design. In his model, a frame spacing of 1.2 meters was used, whereas it is 1.0 meters for the present case, so a reduction of stresses in the present case was expected. 4.15 shows the deflection of the frames suscepted to slamming pressure. The deformations are scaled 100:1.

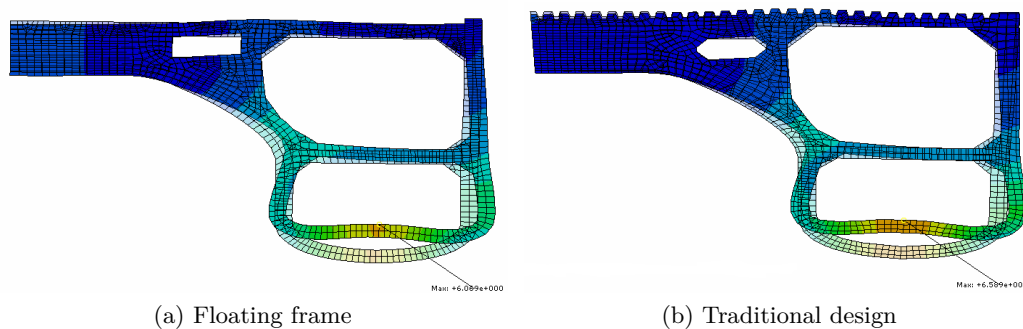(a) Floating frame

(b) Traditional design

Figure 4.15: Comparison of web frame stiffness

It can be seen that the deformation is almost equal for both models, with the floating frame being slightly stiffer than the tranditional frame. This is however to be expected, as the floating frame has a section modulus which is 5.6% higher than that for the traditional frame. The maximum deflections are found to be 6.07 *mm* and 6.59 *mm* for the floating

frame and the traditional frame, respectively. The deflection is thus reduced by 7.9% for the floating frame compared to the traditional frame. This indicates that plating and longitudinal stiffeners in the bottom structure of the floating frame model does contribute to some extent to structural strength of the web frane when suscepted to lateral pressure.
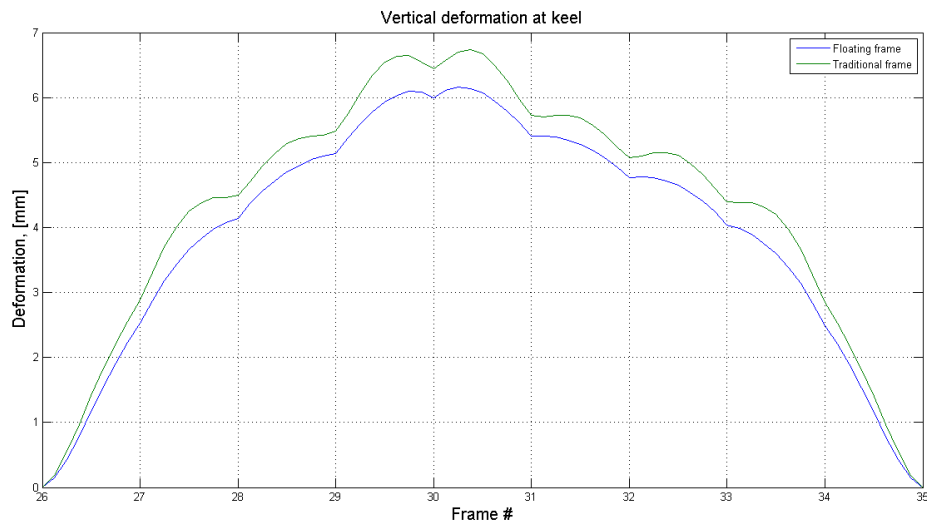

Figure 4.16: Vertical deformation at keel, bottom plating

Figure 4.16 confirms that the floating frame model is stiffer, and that the deformations are very similar, as expected. It should also be noted that the issue of out of plane bending of the longitudinal stiffeners, as discussed in [12] and [11], appears to be resolved by strengthening of the transverse web frames. The highest stresses for the longitudinal stiffeners are found at the connection with the transverse bulkheads with a maximum value as given in table 4.7.

Chapter 5

Fatigue assessment

5.1 Introduction

The DNV HSLC rules provides no specific requirements related to fatigue, thus implying that the fatigue strength may be sufficient when the design loads and strength requirements have been fulfilled. However, DNV HSLC part 3, chapter 9, section 6 states that a number of areas, considered to be critical, are to be considered in a fatigue strength analysis. In general, areas where the dynamic stress level is considered as high, the fatigue strength is to be considered [9].

Furthermore, the fatigue analysis is to be based on a period of time equal to the planned life and usage profile of the craft. The minimum period is 20 years. Cumulative damage due to the stress history may be expressed by linear cumulative damage usage factor. For areas where a potential local failure can be detected before it leads to a critical event, the damage usage factor is not to exceed the value $h = 1.0$. The design criteria specified is to be fulfilled based on S-N data for mean value minus 2 times the standard deviation.

Fatigue is due to cyclic stress variations. There are several sources to such load effects, but those of most interest for the present case are the linear global wave loads and the local pressure variations due to waves. The local wave loads are due to the local sea pressure on the outer plating, and the global stress is due to the behaviour of the ship hull as a beam [13].

In accordance with the DNV HSLC rules, the fatigue criterion, using the Miner-Palmgren approach, can be expressed as:

$$D \approx \sum_i \frac{n_i}{N_i}; \quad N_i \cdot S_i^m = \bar{a} \tag{5.1}$$

$n_i :$ number of cycles in stress range block i
$N_i :$ number of cycles to failure for stress range block i
$S_i :$ applied stress range in block i
$\bar{a}, m :$ geometrical/material parameters

As prescibed in DNV HSLC, the design SN-curve is normally taken as the mean minus two standard deviations curve for relevant experimental fatigue data. This implies that test values exceed the design SN-curve with a 97.7% probability. In general, the fatigue

strength is significantly reduced for increased joint complexity. It is also known that the fatigue performance of welded aluminum structures is reduced compared to unaffected material. Experimental tests have shown that 6082-T6 aluminum welds have a tensile strength of approximately 160-170 MPa compared to circa 270 MPa for the same alloy in an unaffected state [20].

For a JC60 with the floating frame design, as presented in the previous chapters, several areas may be critical in terms of fatigue. In the following sections, only one area will be evaluated. This is the longitudinal stiffener/transverse web frame connection in the bottom structure of the vessel. From chapter 4, relatively high stresses were found at this location, especially for the slamming analysis. The flange-to-flange connection is a rather complex joint, so high stress ranges may prove critical.
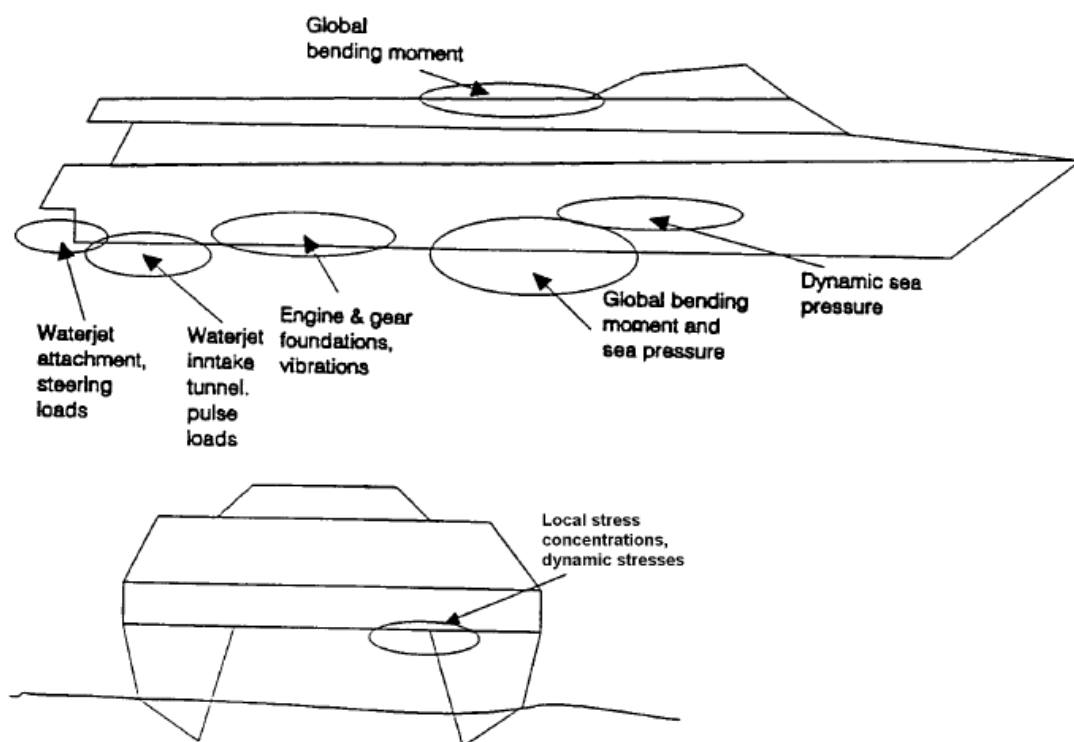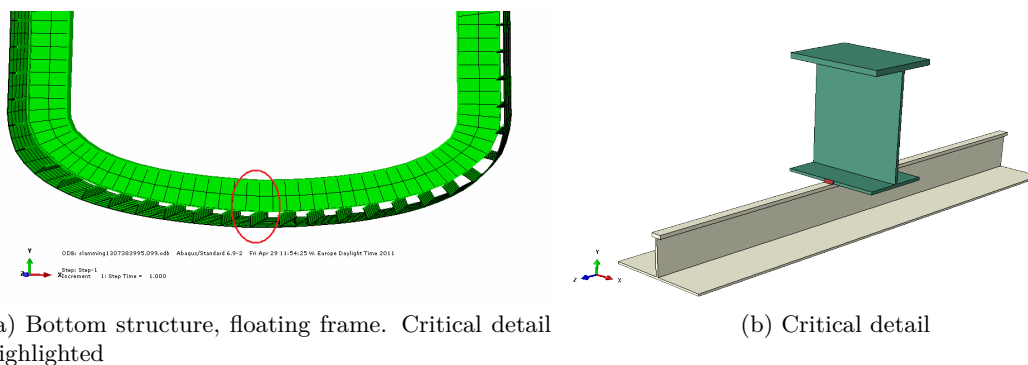

Figure 5.1: Critical areas for fatigue consideration of high speed catamarans, [19].

(a) Bottom structure, floating frame. Critical detail highlighted

(b) Critical detail

Figure 5.2: Structural detail to be evaluated for fatigue strength

Due to the complexity of the structural detail to be examined, it is not immediately obvious where a fatigue crack will have its origin. Three different potential crack initiation sites were identified, and will be evaluated in the following sections. They are labeled HS A, HS B, and HS C, as shown in figure 5.3.
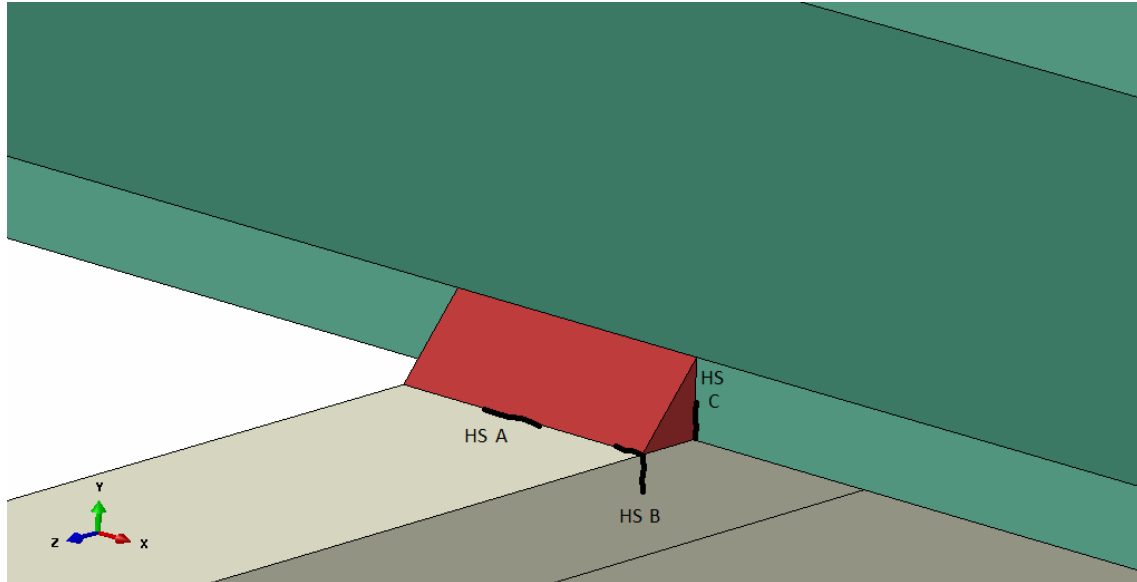

Figure 5.3: Potential crack initiation sites

Eurocode 9 includes classifications of relevant structural details and corresponding SN-curves. In Eurocode 9, HS A, HS B, and HS C corresponds to detail type 3.2, 3.4, and 3.5, respectively.

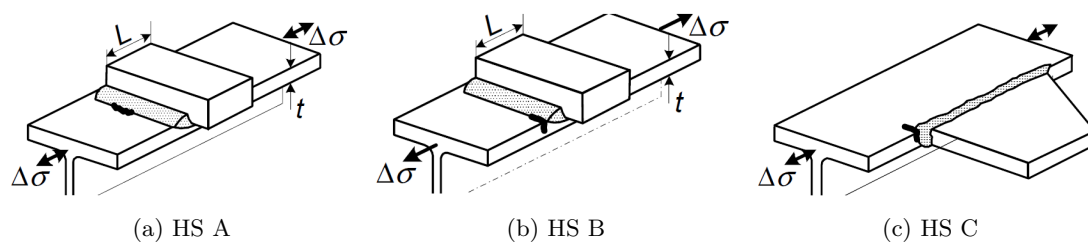| (a) HS A | (b) HS B | (c) HS C |

Figure 5.4: Relevant constructional details, Eurocode 9

To determine the fatigue lifetime of a given structural detail, [19] proposed two different methods named the spectral method and the alternative method. The spectral method is based on analytical and computer analyses, while the alternative method is based on experimental test. The flow chart of the methods is presented in figure 5.5.
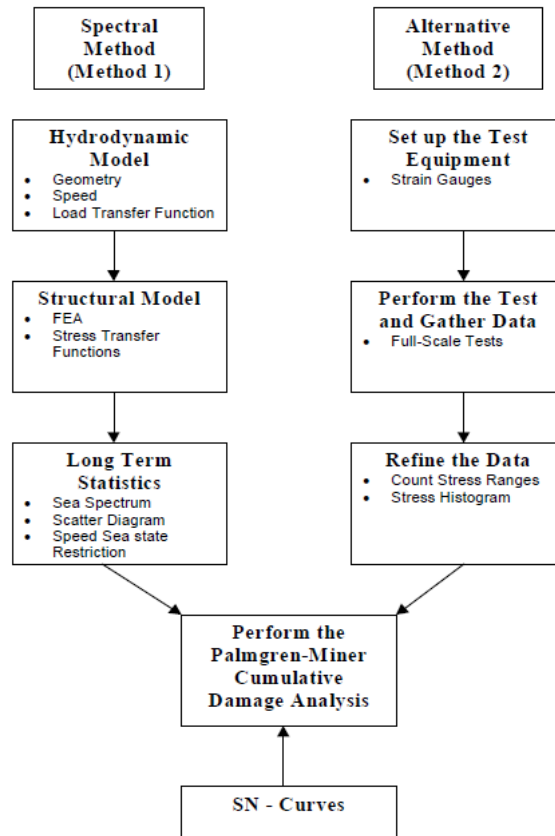
Figure 5.5: Flow chart for fatige analysis, [19].

In the following sections, a simplified version of the spectral method will be presented.

5.2 Development of the loading history

The spectral method requires both hydrodynamic and structural response data to establish the loading and stress transfer functions. The hydrodynamic response of high-speed craft will be provided through a transfer function H as a function of heading θ and wave frequency ω. It defines the loading experienced by the vessel in response to waves. Typical transfer functions include:

$H_v(\omega, \theta)$:	Transfer function for vertical bending moment
$H_h(\omega, \theta)$:	Transfer function for horizontal bending moment
$H_t(\omega, \theta)$:	Transfer function for torsional bending moment
$H_p(\omega, \theta)$:	Transfer function for external pressure

A structural model will utilise the loading information from the hydrodynamic response to develop the corresponding stress coefficients. This can be achieved by developing a finite element model of the ship and subject it to the loading functions of interest. If necessary, local models can be created to determine critical stress coefficients. Stress transfer functions are developed on the basis of the results from the structural analyses. They express the values of a certain stress component resulting from a unit load. The stress coefficient are defined in association with the loading transfer functions:

A_v: Stress per unit vertical bending moment
A_h: Stress per unit horizontal bending moment
A_t: Stress per unit torsional bending moment
A_p: Stress per unit external pressure

The stress history of a detail is normally a function of numerous load components, and they can be linearly summed to develop a combined stress transfer function:

$$H_\sigma(\omega, \theta) = A_v H_v(\omega, \theta) + A_h H_h(\omega, \theta) + A_t H_t(\omega, \theta) + A_p H_p(\omega, \theta) + \ldots \qquad (5.2)$$

Equation 5.2 is used to develop the transfer function of one stress component acting at one area of interest, meaning that a series of combined stress transfer functions is required for a full fatigue analysis.

The short term response is developed by relating the stress transfer function to actual load magnitudes. This is achieved by including the spectral information of the waves to account for the load and stress variations over time. Several wave scatter diagrams and sea sprectra are available. They are to be chosen to correspond to the service route of the vessel. A sea spectrum provides a representation of the waves at a specific, stationary location over time. The sea sprectra are defined by two or more parameters. They are adjusted to best represent a sea state. A commonly used sea sprectrum is the two-parameter Pierson-Moskowitz sea sprectra, defined as:

$$S_\eta(\omega \mid H_s, T_z) = \frac{H_s^2}{4\pi}\left(\frac{2\pi}{T_z}\right)^4 \omega^{-5} \exp\left(-\frac{1}{\pi}\left(\frac{2\pi}{T_z}\right)^4 \omega^{-4}\right) \qquad (5.3)$$

S_η is the sea state, ω the wave frequency, H_s the significant wave height, and T_z the zero crossing period. The probability of occurence for a given sea state is defined in a scatter diagram. The scatter diagram provides a probability p_{ij} for each significant wave height given a zero crossing period and vice versa.

As the wave sprectra refer to a stationary point in the ocean, the given sea spectrum needs to be modified to account for the forward speed of the vessel. The wave encounter frequency, meaning the wave frequency experienced by the vessel, is defined as:

$$\omega_e = \omega\left(1 - \frac{\omega V}{g}\cos\theta\right) \qquad (5.4)$$

V and g are the vessel forward speed and gravitational acceleration, respectively. Accordingly, the sea spectrum is modified:

$$S_\eta(\omega_e) = S_\eta(\omega)\frac{1}{1 - \left(\frac{2\omega V}{g}\right)\cos\theta} \qquad (5.5)$$

For the complete response spectrum, it is normal to account for 'short crestedness' of the seas. This can be achieved through the application of a cosine squared spreading function:

$$S_\eta(\omega_e, \theta) = S_\eta(\omega_e)\cdot\frac{2}{\pi}\cos^2\theta \qquad (5.6)$$

The response spectrum, for a given combination of H_s, T_z, and θ, is then given by:

$$S_\sigma\left(\omega \mid H_s, T_z, \theta\right) = \left|H_\sigma\left(\omega \mid \theta\right)\right|^2 \cdot S_\eta\left(\omega_e, \theta \mid H_s, T_z\right) \tag{5.7}$$

The moments for the stress spectrum for the ith sea state and jth heading:

$$m_{kij} = \sum_\infty \omega^k S_\sigma\left(\omega \mid H_s, T_z, \theta\right) \mathrm{d}\omega \tag{5.8}$$

where m_{kij} is the kth moment. The short term stress range distribution for the ith sea state and jth heading is defined as:

$$F_{\Delta\sigma ij}(\sigma) = 1 - \exp\left[-\frac{\sigma^2}{8m_{0ij}}\right] \tag{5.9}$$

The corresponding zero crossing frequency is given by:

$$v_{ij} = \frac{1}{2\pi}\sqrt{\frac{m_{2ij}}{m_{0ij}}} \tag{5.10}$$

It is here assumed that the variation of stresses in a short-term sea state is a narrow banded, random process. As fatigue and damage tolerance represent long-term events, it is necessary to extrapolate the data to reflect long-term behaviour and response. The long-term extreme response can be found by summation of the short-term responses over a given period of time. This results in a probability density function for long-term distribution defined by:

$$f\left(\sigma_a\right) = \frac{\sum_i \sum_j n_* p_i p_j f_*\left(\sigma_a\right)}{\sum_i \sum_j n_* p_i p_j} \tag{5.11}$$

$\sigma_a = $ Stress amplitude
$f_* = $ Probability density function for short-term response
$n_* = $ Average number of responses per unit time, short-term response
$p_i = $ Weighting factor for the ith sea state
$p_j = $ Weighting factor for the jth heading

The total stress range distribution is finally given by:

$$F_{\Delta\sigma} = \sum_i \sum_j r_{ij} F_{\Delta\sigma ij}(\sigma) p_{ij} \tag{5.12}$$

$p_{ij} = $ The probability of occurence of a given sea state and heading.
$r_{ij} = \frac{v_{ij}}{v_0}$ The weighted function that consists of the crossing rate in a given sea state and the average crossing rate.
$v_0 = p_{ij}v_{ij}$ The average crossing rate.

As no evaluation of the load spectra, as defined above, has been performed, an approximation of the long-term distribution of stress maxima is needed. [3] and [13] suggested to model the long-term distribution as a two-parameter Weibull distribution:

$$S = S_0 \left[1 - \left(\frac{\log n}{\log n_0} \right) \right]^{\frac{1}{\xi}} \tag{5.13}$$

Where:

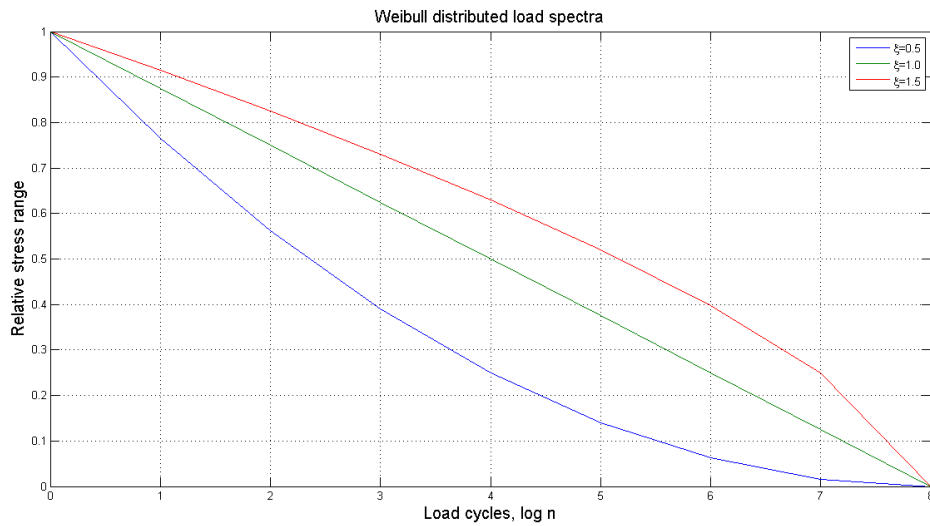|		
$S_0 =$		Maximum stress range in the load history.
$n =$		Number of load cycles exceeding S.
$n_0 =$		Total number of load cycles in the load history.
$\xi =$		Weibull shape parameter.

Figure 5.6: Exceedances of stress ranges represented by the Weibull distribution with different shape parameters

For determination of the cumulative fatigue damage, the Miner sum can be calculated by two different methods, depending on the SN-curve used. If the basic SN-curve is used, $\bar{a} = N_{ref} \cdot S_{ref}^m$, the cumulative fatigue damage can be calculated as [13]:

$$D = \sum_i \frac{n_i}{N_i} = \frac{n_0}{\bar{a}} \cdot (2\lambda)^m \cdot \Gamma \left(1 + \frac{m}{\xi} \right) \tag{5.14}$$

Where λ is the Weibull scale parameter and Γ is the complete Gamma function. However, if a SN-curve different from the basic SN-curve is to be applied, the Miner summation can be performed by subdividing the load spectra into stress range blocks, as shown examplified in figure 5.7.
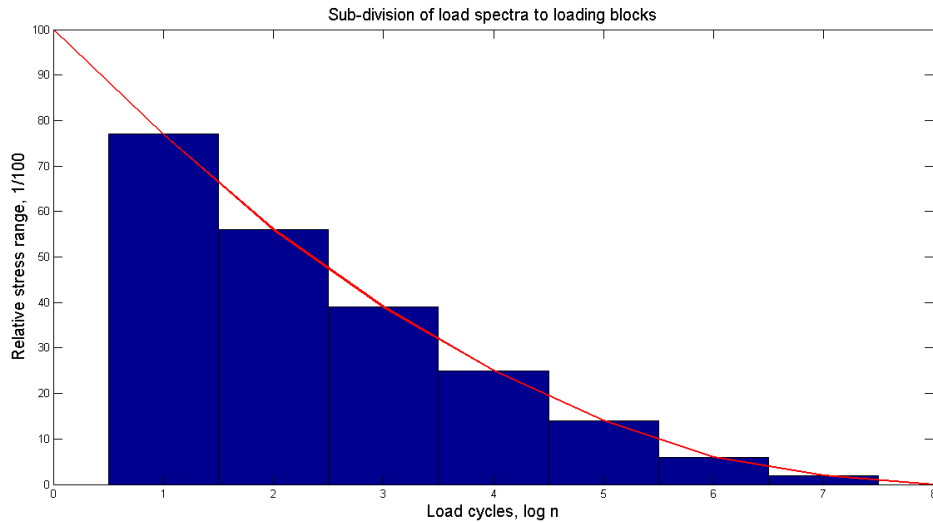
Figure 5.7: Example of sub-division of load spectra to stress range blocks

Obviously, the choice of Weibull parameters is very important for the evaluation of fatigue strength. It can be seen from equation 5.14 that the cumulative fatigue damage is sensitive to changes of the Weibull distribution parameters. [12] estimated the shape parameter $\xi = 0.8$. In [13], Heggelund performed a case study of a 120 meter catamaran. At the location equivalent to the present case, he found the parameters to have different values depending on the response levels considered. For the total range of response levels, he found $\xi = 0.90$ and $\theta = 1.37$, while $\xi = 0.81$ and $\theta = 1.19$ were found for the response levels most relevant for fatigue damage. The cumulative fatigue damage was found to be 13.5% higher for the data set with the most relevant response levels compared to the full data set. For the present case, the following values will be used:

Shape parameter, $\xi =$	0.81
Worst case, $\xi_{WC} =$	0.90

Another important consideration is the total number of load cycles. For 20 years service, which is the minimum period (see section 5.1), the total number of load cycles is often set to $n_0 = 1 \cdot 10^8$. In [13], it was assumed that a large passenger ferry would have 6700 operating hours per year, e.g. it would be in operation 76.5% of the time in its lifetime. Subsequently, he found that n_0 was in the range $1.6 - 1.8 \cdot 10^8$. For the present case, this appears overly conservative. The total number of load is set to $n_0 = 1 \cdot 10^8$, which is still considered a conservative estimate for the present case. The long term stress distribution used for the following analyses is presented in figure 5.8.
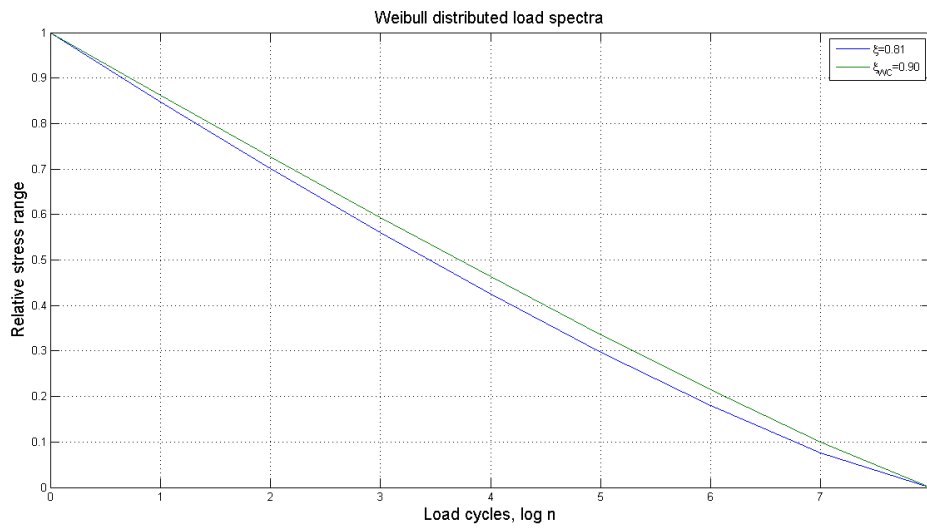
Figure 5.8: Load spectras

Fatigue desing codes for aluminum structures using stress range and SN-curves can be based on a nominal stress range approach or a hot spot stress range approach. Finite element analysis will be used to determine the maximum stress range. For the present case, this is assumed to occur when the vessel is subjected to symmetric bottom slamming (see section 2.2.1). The relevant stresses is determined by applying the loads, stresses and displacements found from the web frame analysis discussed in section 4.4 to a local model as shown in figure 5.2b.

5.3 Finite element models

For the development of a local model, the boundary conditions need to be applied in a manner such that the local model is compatible with the global model. For the bottom longitudinal stiffener-transverse web frame connection, as illustrated in figure 5.2, the web frame slamming analysis indicated symmetry about the vertical neutral axis. This is shown in figure 5.9, displaying a contour plot of the equivalent stress at the given location.
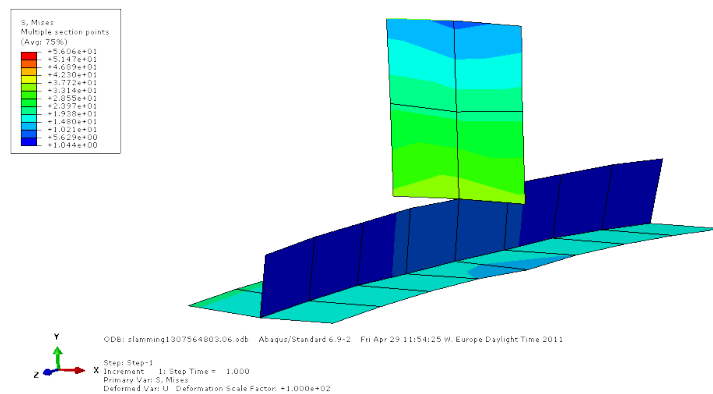

Figure 5.9: Equivalent stress for bottom stiffener-transverse web frame connection, slamming analysis.

In the real structure, the area of interest is slightly curved about the longitudinal neutral axis. For simplicity, this curvature is neglected in the modelling. It is assumed that this simplification has little impact on the local structural behaviour of interest at the potential crack initiation sites, illustrated in figure 5.3.

The transverse web frame experiences in-plane bending due to the slamming load. From the slamming analysis results, it is found that the bending stress for the transverse web frame varies linearly over the height of the web frame. At the cross sectional neutral axis, the bending stress is close to zero, indicating that the bending stress is almost exclusively due to the slamming induced transverse bending moment and that axial forces in the web frame at the given location are close to zero.

From the slamming analysis, bending stresses of -55,4 MPa (compression) and 38.0 Mpa (tension) are found at the bottom and upper flange of the transverse web frame at the given location. By $M_{bend} = \sigma_{bend}Z$, the bending moment is found to have a value of $M_{bend} = 26.2$ kNm. In the modelling, this bending moment was added by applying six sets of concentrated forces, three above the cross sectional neutral axis and three below, as shown in figure 5.10. The concentrated forces were applied at locations approximately 1/3, 2/3, and 3/3 of the distance from the neutral axis to the top/bottom flange. Also the magnitudes of the forces varied linearly with the height of the web frame, from -60.1 kN at the bottom flange to 40.3 kN at the top flange.
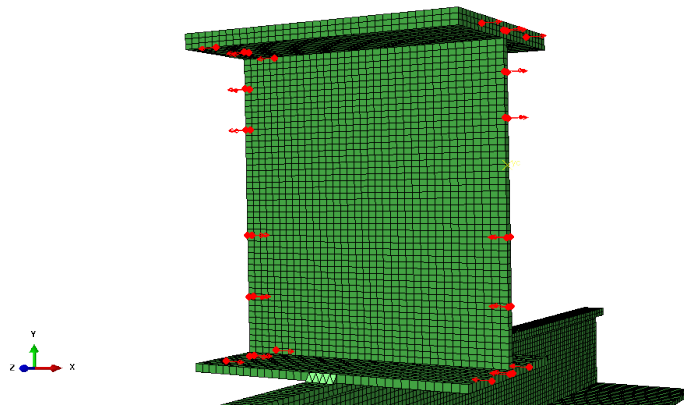

Figure 5.10: Concentrated forces applied to web frame to replicate bending moment.

The same slamming load as used for the transverse web frame slamming analysis is used for the local model, i.e. an evenly distributed pressure acting on the bottom plating, $p_{sl} = 82.3$ kN/m^2. This vertical load is mainly carried by the transverse web frame, so springs acting in vertical direction were added to all nodes at the cross sectional faces of the transverse web frame, shown as purple objects in figure 5.11.
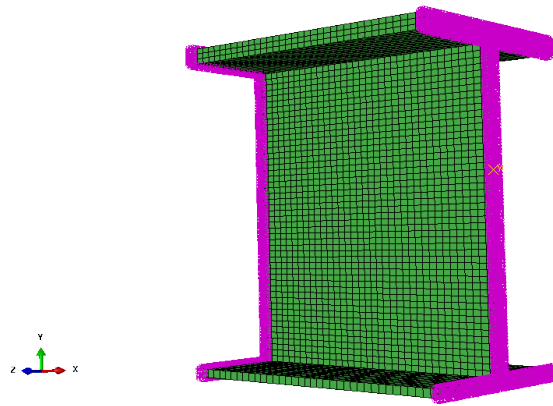
Figure 5.11: Springs acting in vertical direction to carry slamming load
.

This modelling induces an additional bending moment to the transverse web frame. Assuming that the web frame (in this case) can be considered a simply supported beam and that the slamming load transferred via the longitudinal stiffener to the web frame can be idealized as a concentrated force, the induced bending moment may be taken as $M = \frac{F_{slam}L_{frame}}{4} = 0.96$ kNm, merely 4% of the applied bending moment.

Although horizontal forces acting on the models, i.e. the concentrated forces acting on the web frame, should be balanced, any imbalance will be absorbed by the symmetry boundary conditions at the edges of the bottom plate. The contact in the area between the welds has been modelled as a frictionless surface-to-surface contact, which is assumed to resemble the actual contact in a satisfying manner.

In [8], DNV suggests two methods of modelling. The simplest way of modelling is offered by shell elements arranged in the mid-plane of the structural components. 8-noded elements are recommended in the case of steep stress gradients. A mesh size from txt up to 2tx2t may be used. For the hot spot region, txt is preferred. The second method, more suitable for complex cases, is offered by solid elements, preferably isoparametric 20-node elements. Again, element length corresponding to plate thickness is recommended and no larger than 2 t. Furthermore, the fillet weld should be modelled to achieve proper local stiffness and geometry.

Four different finite element models has been created in ABAQUS CAE, version 6.10.2. The all have the same main characteristics and material properties, and loads and boundary conditions are applied as stated above. What separates them is the elements used in the modelling, the refinement of the mesh, and the weld modelling. They are labeled models 1-4.

Model 1 is constructed by 8-node shell elements, reduced integration (S8R), in accordance to [8]. Element sizes vary between 5.5mm x 5.5mm to 6.0mm x 6.0mm. The relevant plate thicknesses are 10.0mm for the stiffener flange and 8.0mm for the web frame bottom flange. This means that the mesh is slightly more refined than what is recommended. No weld is modelled for this model, and since the shell elements are arranged in the mid-plane of the structural components, a tie-constraint was needed to join the stiffener and the web frame. For this constraint, it is necessary to establish a master-slave relationship for the nodes. Generally, the nodes for the loaded structure are assigned as master nodes. For the present case, where both structural elements are loaded, it was not obvious which set of

nodes that should be assigned as master nodes. However, analyses proved that the results were practically unaffected by the choice of master nodes.
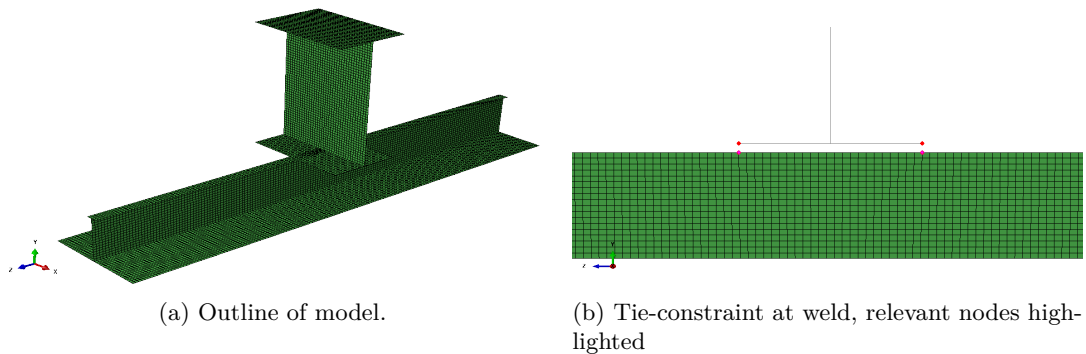

(a) Outline of model.

(b) Tie-constraint at weld, relevant nodes highlighted

Figure 5.12: Model 1

Model 2 is contructed by 20-node solid elements with reduced integration, termed C3D20R in ABAQUS. The element length vary between 5.0mm to 8.0 mm, where two elements is modelled over the stiffener flange thickness and one element over the web frame bottom flange thickness. For this model, no weld has been modelled, the stiffener and web frame are thus connected through merging of nodes at the weld root, as illustrated in figure 5.13b. Model 2 is also in accordance with the recommendation given in [8], except for the fillet weld, that has not been modelled.

(a) Outline of model.
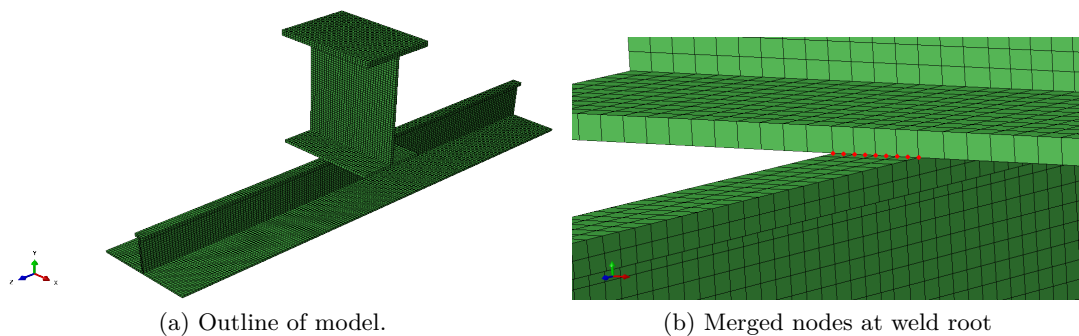
(b) Merged nodes at weld root

Figure 5.13: Model 2

Model 3 is equal to Model 2, but this model has an idealised weld included. The weld covers the full thickness of the web frame bottom flange thickness, i.e. a leg length of 8mm, while the horizontal leg length is 5mm. The element type used for the weld is ten node tetrahedral elements, termed C3D10. In general, tetrahedral elements are inferior to hexahedral elements in terms of accuracy for a finite element analysis, so the stresses at the interface for these elements may be inaccurate. However, the load transfer should be correct. No weld fusion has been modelled, nodes at the legs has simply been merged, as illustrated in figure 5.14b.

(a) Weld fusion

(b) Weld idealisation. Merged nodes at stiffener flange and web frame bottom flange highlighted.
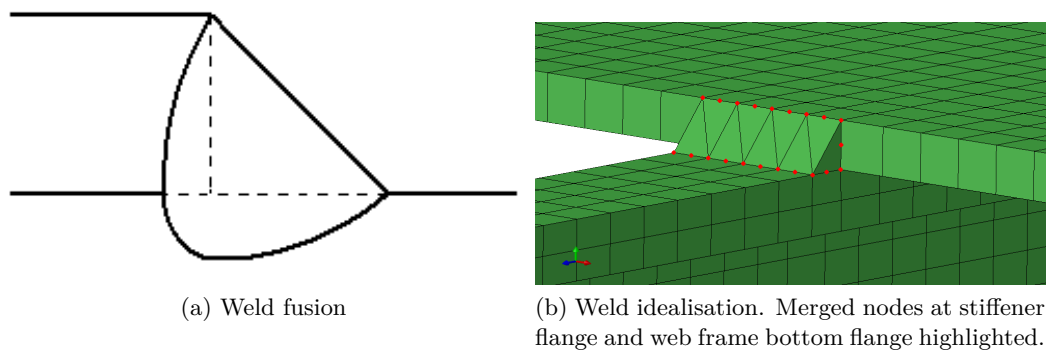
Figure 5.14: Model 3

Model 4 is constructed exclusively by 4-node tetrahedral elements (C3D4). The weld is idealised as a triangular prism where both leg lengths are 8mm. As for Model 3, no weld fusion is included in the model, and the interaction between the structural elements is equal for Model 3 and 4. However, Model 4 has a fine mesh at the hot spot region, with a characteristic element length of approximately 2mm. For the rest of the model, an element length of 8mm is applied.
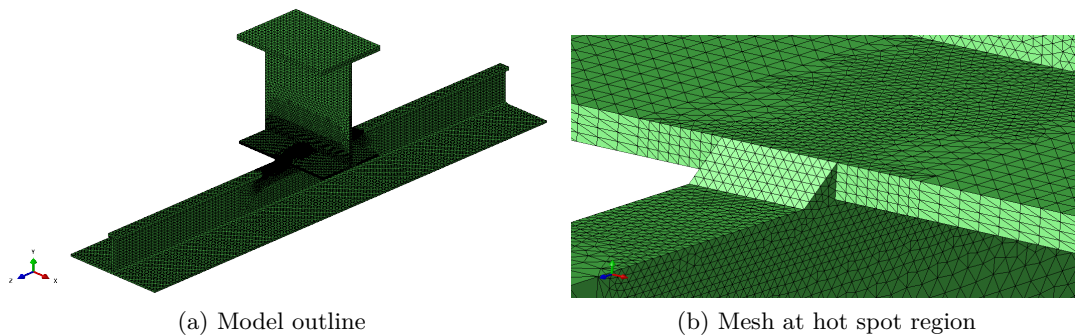

(a) Model outline

(b) Mesh at hot spot region

Figure 5.15: Model 4

5.4 Calculation of fatigue damage

For determination of the cumulative fatigue damage, the nominal stress range approach will be applied. For this approach, the design stress is the local nominal stress range, which does not include stress raisers due to local weld geometry or local geometrical changes. This implies that effects from structural discontinuity and local notch effects are implicitly included in the fatigue strength curves, i.e. the SN-curves. The Eurocode 9 fatigue design code is based on the nominal stress range approach, and will be used as basis for the following calculations.

Three constructional details, shown in figure 5.4, has been identified as the equivalent for the potential crack initiation sites, illustrated in figure 5.3. These contructional details are categorised in detail category 23-3.4, 20-3.4, and 18-3.4 for HS A, B, and C, respectively. The detail categories are labeled according to their characteristic stress range, S_{ref}, which is the stress range at $N_{ref} = 2 \cdot 10^6$ cycles. The corresponding SN-curves are shown in figure 5.16.
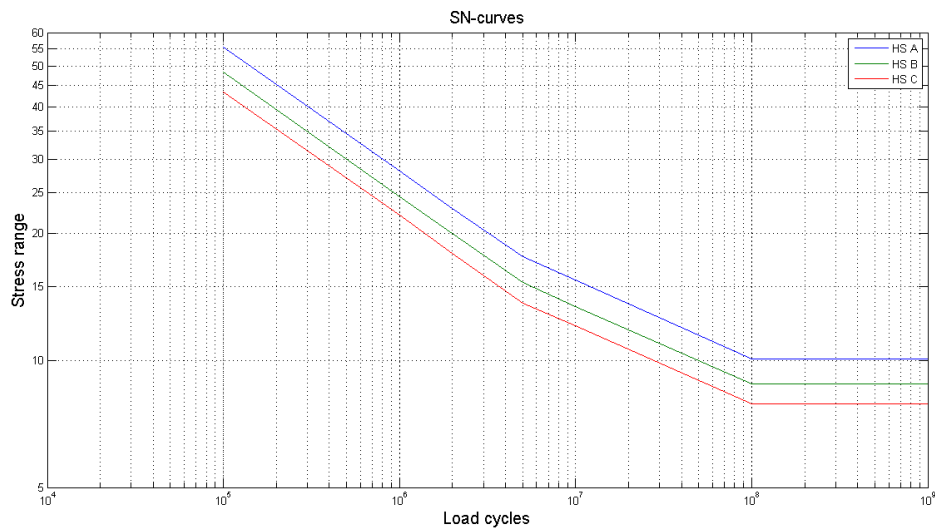
Figure 5.16: SN-curves to be used for the cumulative fatige damage calculation.

The design stress range to be used with the SN-curves above is the nominal stress range at the initiation site. It is stated in [4] that where the axial stress distribution is linear across the member section about both axes, the stresses at the initiation point may be used directly. This is not the case at the hot spot regions. The nominal stress needs to be estimated by other means, as will be presented for HS A, B, and C in the following sections.

5.4.1 HS A

Figure 5.17 shows the longitudinal bending stress (the stress component normal to the weld) at the surface along the stiffener flange centerline for the four local models. It is seen that the stresses are within close range of eachother from the end upto about 30mm (3 times stiffener flange thickness) from the weld root. Close to the weld root, the stresses differ significantly. This is due to the presence of weld and structural discontinuity and how these structural details are modelled in the different models.
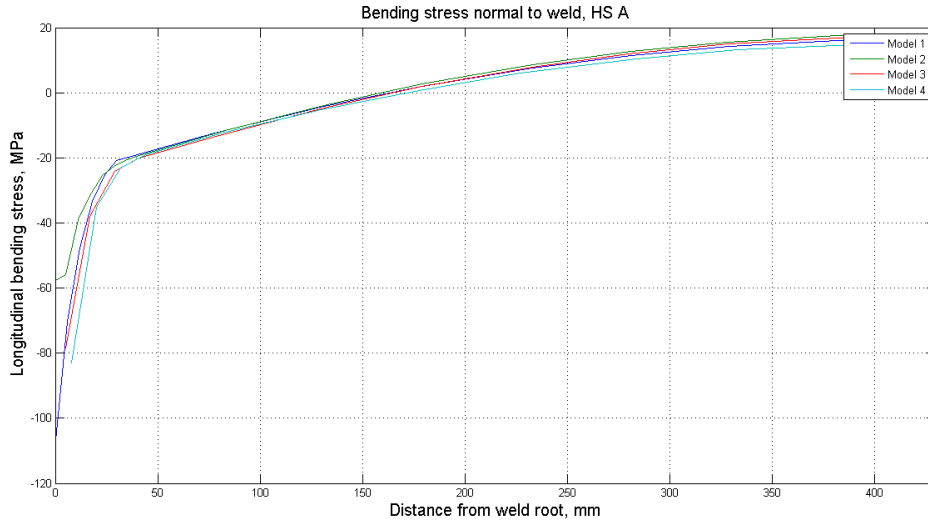

Figure 5.17: Bending stress normal to weld along horizontal line at center of stiffener flange

In the area where the stress raisers at the weld do not contribute, it is seen that the bending stresses increase close to linearly. It is thus assumed that the nominal stress at the HS A may be found be linear extrapolation. At a distance 80mm from the weld root, a mean stress of -12.5 MPa is found for the four models. Likewise, a mean stress at a distance 30mm from the weld root is found to have a value of -22.5 MPa, so linear extrapolation yields a nominal stress of -28.5 MPa at the weld root. The stress at the weld root is used instead of the stress at the weld toe to ensure conservativeness as the stress estimate may be inaccurate.

It is assumed that the extreme stress range goes from zero to the extreme nominal stress, so the maximum stress range in the load history is thus $S_0 = 28.5$ MPa. With the Weibull parameters as given in section 5.2, the long term cumulative load distribution is as shown in figure 5.18.
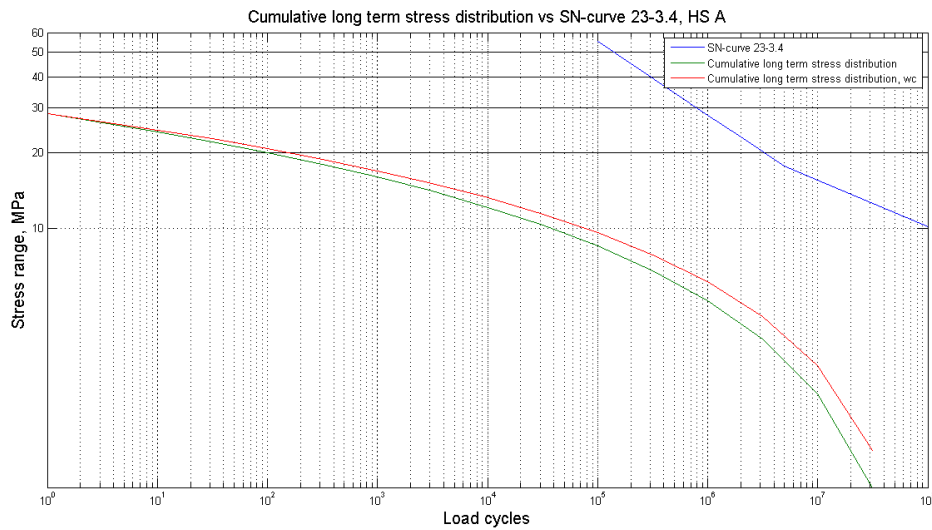
Figure 5.18: Cumulative long term distribution of stresses and corresponding SN-curve

The relevant SN-curve for HS A, 23-3.4, has a cut-off limit at 10.1 MPa, meaning that stresses below this level does not contribute to fatigue damage. It is seen that approximately $4 \cdot 10^4$ load cycles will contribute to fatigue damage for the estimated Weibull shape parameter, while the worst case Weibull shape parameter will have approximately $8 \cdot 10^4$ load cycles contributing to fatigue damage.

The Miner sum is found by subdividing the cumulative long term stress distribution into a stress range blocks with load cycle intervals ranging from 10^2 to 10^3 for stress ranges exceeding the cut-off limit. The number of load cycles in the stress range block is divided by the corresponding number of load cycles to failure. By summation of all these contributions to fatigue damage, the cumulative damage for HS A is:

$$
\begin{aligned}
D &= 4.11 \cdot 10^{-3} \\
D_{WC} &= 5.22 \cdot 10^{-3}
\end{aligned}
$$

Given a fatigue criterion of $D = 1.0$, it is reasonable to assume that HS A is not critical in terms of fatigue. The worst case Weibull shape parameter yields an increase of approximately 27% for the cumulative fatigue damage.

5.4.2 HS B

To determine the nominal stress at HS B, the same method as in section 5.4.1 is applicable. The longitudinal bending stress at the edge of the stiffener flange is shown in figure 5.19
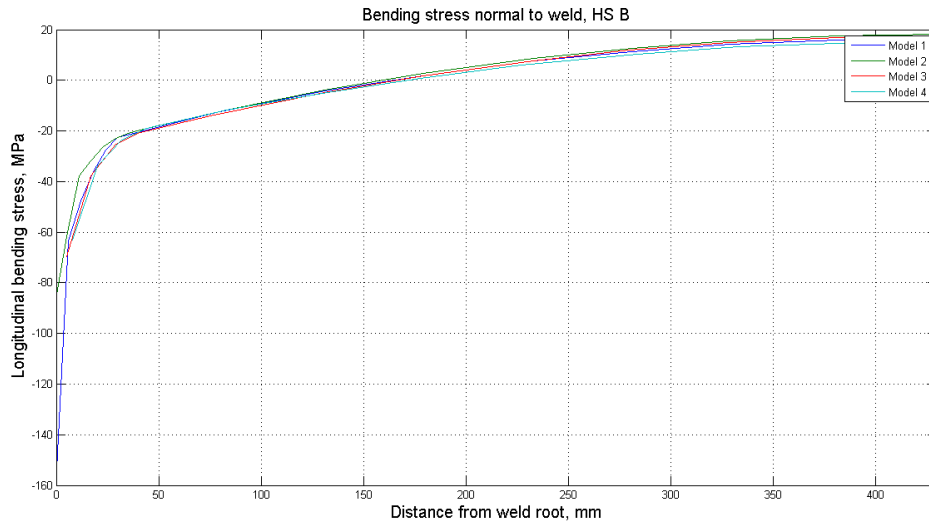

Figure 5.19: Bending stress normal to weld along horizontal line at edge of stiffener flange

The stresses at the edge of the stiffener flange are similar to those at the center of the flange, discussed in section 5.4.1. Accordingly, the bending stress at the weld root is determined by linear extrapolation, yielding a extreme nominal stress of 29.3 MPa. In this case, as for the case for HS A, the maximum stress range in the load history is thus set to 29.3 MPa. The long term cumulative load distribution is as shown in figure 5.20.
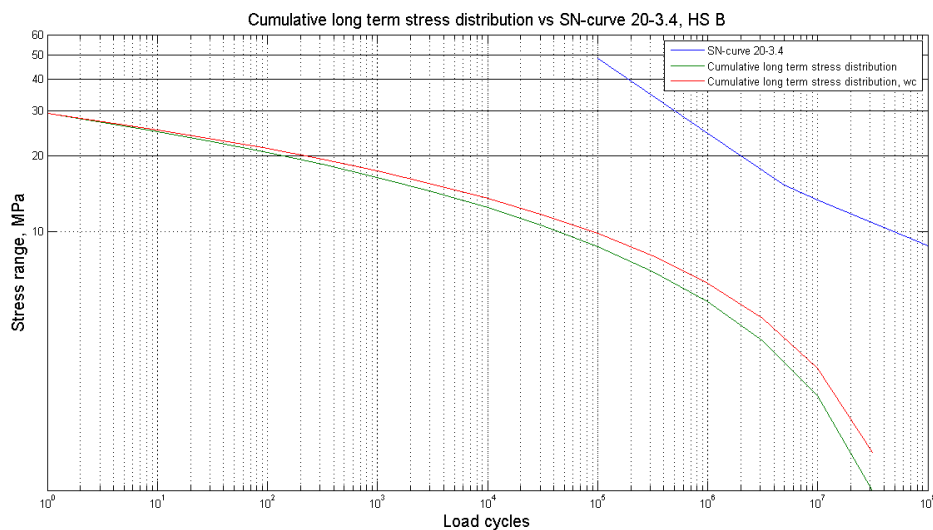

Figure 5.20: Cumulative long term distribution of stresses and corresponding SN-curve

The corresponding SN-curve is termed 20-3.4, with a cut-off limit of 8.8 MPa. For the given cumulative long term stress distributions, approximately $1 - 2 \cdot 10^5$ load cycles

will contribute to fatigue damage. By Miner summation, as performed for HS A, the cumulative fatigue damage is:

$$D = 7.92 \cdot 10^{-3}$$
$$D_{WC} = 1.04 \cdot 10^{-2}$$

The results indicate that HS B is not critical. For the worst case Weibull shape parameter, the cumulative fatigue damage is increased by 32% compared to the estimated Weibull shape parameter. It is seen that the cumulative fatigue damage for HS B is almost doubled compared to that for HS A.

5.4.3 HS C

The transverse bending stresses at the web frame bottom flange edge is found to vary significantly for the different models, and the results from the analyses are inconsistent, as seen in figure 5.21. A possible explanation is the modelling of the bending moment by concentrated forces distributed over the cross section of the web frame. Very high local stresses are found at the locations where the concentrated forces act, and these propagate to the surrounding area, thus causing disturbances in the stress distribution.
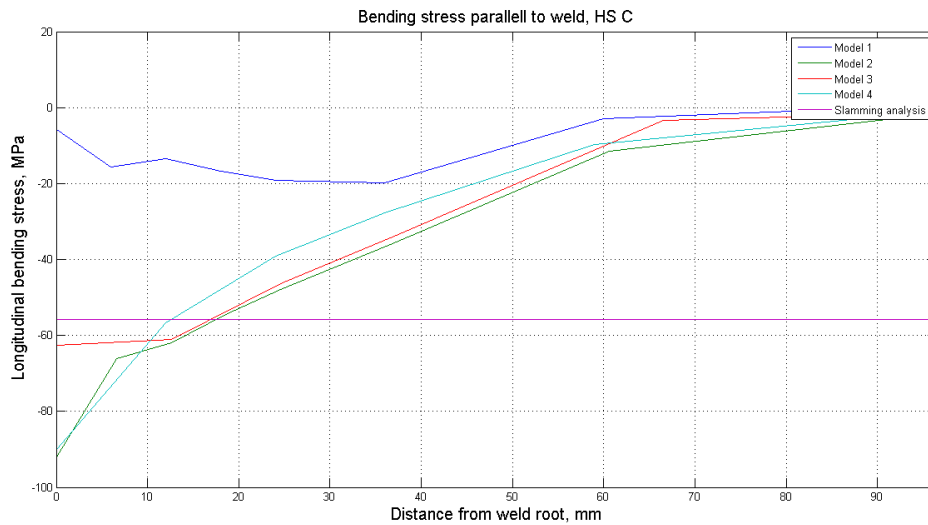

Figure 5.21: Bending stress parallell to weld along horizontal line at edge of web frame bottom flange flange

The transverse bending stress from the slamming analysis has a value of -55.4 MPa at the same location. This is seen to correspond to the stresses found for models 2 and 3 about 16mm from the weld root, equal to two times the plate thickness for the web frame bottom flange. The extreme nominal stress is taken as the stress from the slamming analysis, and the corresponding maximum stress range in the load history is thus taken as $S_0 = 55.4$ MPa. The cumulative long term distributions of stresses are subsequently as shown in figure 5.22.
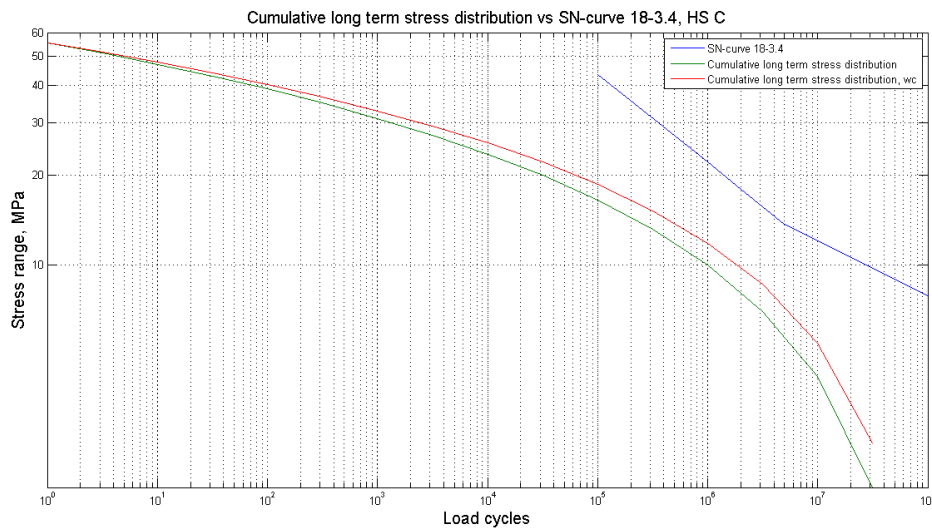
Figure 5.22: Cumulative long term distribution of stresses and corresponding SN-curve

The corresponding SN-curve 18-3.4 for HS C has a maximum stress range of 43.4 MPa with the correponding number of cycles to failure of $N = 1 \cdot 10^5$. It is assumed that the SN-curve may be extrapolated upto a stress range of 85.5 MPa, where the corresponding number of cycles to failure is $N = 1 \cdot 10^4$. By subdividing the cumulative stress distribution into a finite number of stress blocks and performing Miner summation, the following cumulative fatigue damages are found:

$$
\begin{aligned}
D &= 3.52 \cdot 10^{-1} \\
D_{WC} &= 5.66 \cdot 10^{-1}
\end{aligned}
$$

For a fatigue criterion of $D = 1.0$, the results indicate that excessive fatigue damage will not occur at HS C. However, the cumulative fatigue damage for HS C is far higher than for HS A and HS B, indicating that HS C is the most critical hot spot region. Although a series of assumptions and simplifications has been made in the calculations, it is reasonable to believe that they are conservative. Consequently, a critical fatigue failure at HS C appears unlikely.

Chapter 6

Conclusions

A modified version of the JumboCat 60 with floating transverse web frames has been evaluated from a strength perpective with focus on hull beam strength, local structural response due to extreme loading, and fatigue of a structural detail in the bottom structure of the vessel.

Using the DNV HSLC rules, it is found that the modified JC60 fulfils the minimum requirements related to scantlings. Furthermore, the design loads are shown to be equal for the floating frame version and the original version of the JC60.

The structural response for two global and one local load condition has been evaluated by finite element analysis for the floating frame version and the traditional version of the vessel. For the local slamming load condition, no stresses exceeding the allowable stress levels defined by DNV HSLC rules are found. By comparing the floating frame model and the traditional model, it is seen that the floating frame model is slightly stiffer for this particular load condition. It was also shown that the high stres concentrations found by Jon Englund and Toralf Ervik, especially at the longitudinal stiffener webs due to out-of-plane bending, was significantly reduced by strengthening of the transverse floating frame.

The global torsional/pitch connecting moment load condition also showed stress levels within the allowable. It was indicated by the results that the traditional model had a higher hull beam torsional stiffness than the floating frame model. The transverse bending moment load condition indicated that the original model hull beam was stronger in transverse direction than the floating frame model. For this analysis, local stress concentrations were found to have stress levels exceeding the allowable. As the stresses for the floating frame model were found to exceed those of the traditional model, it is suggested that the plate thickness of the bottom plating at a specified area is increased for the floating frame version. Also, the results from the transverse bending analysis indicated high shear stresses were found for the longitudinal stiffeners at the transverse bulkheads for the floating frame model. In order to reduce these stresses, it is suggested that at least the stiffeners in the critical area have their dimensions increased in order to increase their shear area.

The fatigue strength of the longitudinal stiffener/transverse web frame connection in the bottom structure of the floating frame version was investigated. The cumulative fatigue damage for three different hot spot areas was calculated by Miner summation. A Weibull distributed cumulative long term distribution of stresses, using a shape parameter of $\xi =$

0.81 and a total number of load cycles of $1 \cdot 10^8$ for 20 years of service, was combined with SN-curves given in Eurocode 9 in the Miner summation. The design stress was the nominal stress at the crack initiation site. This was estimated using the results from finite element analysis using four different local models of the structural detail, and the local slamming finite element analysis. For the hot spot areas at the stiffener flange, the cumulative fatigue damage was found to be in the region $D = 4.1 \cdot 10^{-3} - 1.0 \cdot 10^{-2}$, while at the transverse web frame bottom flange, the cumulative fatigue damage was estimated to be in the range $D = 0.35 - 0.57$. The fatigue criterion was assumed to be $D = 1.0$, meaning that the structural detail evaluated is considered non-critical in terms of fatigue.

6.1   Recommendations for further work

As this thesis only studies the structural response for three load conditions, it is suggested that the remaining load conditions, as defined in DNV Classification Notes 30.8, are evaluated for the floating frame version of the JumboCat 60. Linear and non-linear local analyses should be performed as seen appropriate, for example at the critical area termed region 1 in the tranverse bending moment analysis.

A calculation of the hydrodynamic loads on the vessel would be useful to estimate the actual global and local wave loads. These loads could in turn be used to determine the global and local structural response more realistically than by the idealised loads applied in the analyses presented in this thesis. A complete hydrodynamic analysis could also serve as basis for calculation of the long term distribution of stresses used in fatigue calculations.

For a complete fatigue assessment, several other structural details other than the one presented in this thesis need to be evaluated. Lab tests investigating the fatigue strength of relevant structural details would be useful to develop SN-curves suited for the floating frame design.

The increase of hull weight due to the use of floating frames should be calculated in order to determine the life cycle costs for the floating frame desing compared to the original design. It is in this case relevant to investigate if the reduced building cost compensates for a potential increase in fuel consumption due to increased hull weight.

Bibliography

[1] A. Aalberg. Redningsselskapets skøyte 'knut johan' - konstruert med stivere liggende utenpå spantprofiler. Technical report, Norwegian University of Science and Technology, NTNU, 2006.

[2] J. Amdahl. Vurdering av lokalkrav til plater og stivere i ulike standarder for småbåter i aluminium. Technical report, Norwegian University of Science and Technology, NTNU, 2006.

[3] S. Berge. Fatigue design of welded structures, September 2006.

[4] CEN. *Eurocode 9: Design of aluminum structures - Part 1-3: Structures susceptible to fatigue.* European Commitee for Standardization, May 2007.

[5] DNV. *Classification Notes No. 30.8, Strength Analysis of Hull Structures in High Speed and Light Craft.* Det norske Veritas, August 1996.

[6] DNV. *Rules for Classification of High Speed, Light Craft and Naval Surface Craft, Part 3, Chapter 3, Hull Structural Design, Aluminum Alloy.* Det norske Veritas, July 2000.

[7] DNV. *Rules for Classification of High Speed, Light Craft and Naval Surface Craft, Part 3, Chapter 1, Design Principles, Design Loads.* Det norske Veritas, January 2005.

[8] DNV. *Recommended Practice DNV-RP-C203, Fatigue Design of Offshore Steel Structures.* Det norske Veritas, April 2010.

[9] DNV. *Rules for Classification of High Speed, Light Craft and Naval Surface Craft, Part 3, Chapter 9, Direct Calculation Methods.* Det norske Veritas, January 2011.

[10] J. Englund. Finit element-analys av knut johan. Unpublished, 2009.

[11] J. Englund. Structural strength of work boats and high speed crafts with floating frames. Master's thesis, Kungliga Tekniska högskolan, KTH, 2009.

[12] T. Ervik. Structural strength of work boats and high speed crafts with pre-fabricated, floating panels in aluminium. Master's thesis, Norwegian University of Science and Technology, NTNU, 2010.

[13] B.W. Tveiten Heggelund, S.E. and T. Moan. Fatigue analysis of high speed aluminum catamarans. In *The Third International Forum on Aluminum Ships*, 1998.

[14] S.E. Heggelund and T. Moan. Analysis of global load effects in catamarans. *Journal of Ship Research*, 2001.

[15] T. Moan Heggelund, S.E. and S. Oma. Global structural analysis of large catamarans. In *Proc. Fifth International Conference on Fast Sea Transportation, FAST'99*, 1999.

[16] P.D. Herrington and R.G. Latorre. Development of an aluminum hull panel for high-speed craft. *Marine Structures*, 1998.

[17] P.D. Herrington and R.G. Latorre. Development of a high-speed aluminum ferry with floating frames. Technical report, University of New Orleans, 2000.

[18] O.D. Økland. Analysis of transverse section of the 60m jumbo cat. Technical report, Marintek, 1999.

[19] B. Rampolla Kramer, R.K. and A. Magnusson. Fatigue of aluminum structural weldments. Technical report, Ship Structure Committee, May 2000.

[20] S. Missori and A. Sili. Mechanical behaviour of 6082-t6 aluminum alloy welds. *Metallurgical Science and Technology*, 1999.

[21] L.J. Mong. Konstruksjonsstyrke til bruksbåter og hurtiggående båter med prefabrikkerte, utenpåliggende paneler i aluminium. Technical report, Norwegian University of Science and Technology, NTNU, 2010.

[22] USS. Steel vs. aluminum: The basics. `http://xnet3.uss.com/auto/steelvsal/basicfacts.htm`, January 2011.